

Robust Filter Attention: Self-Attention as a Parallel State Estimator

Peter Racioppo¹

Abstract

We introduce Robust Filter Attention (RFA), an attention mechanism that reformulates self-attention as parallel robust filtering under a latent stochastic differential equation (SDE) prior, where analytically propagated uncertainty defines a time-dependent precision prior over attention weights. This formulation integrates key advantages of existing positional encodings: it preserves RoPE-style rotational structure while achieving long-context stability through explicit modeling of dissipation and diffusion. By imposing isotropic constraints on the dynamics and noise, RFA matches the $\mathcal{O}(N^2d)$ time and $\mathcal{O}(N^2 + Nd)$ memory complexity of standard attention. Empirically, we find that uncertainty-aware weighting induces specialization into distinct filtering regimes across heads, improving temporal consistency and extrapolation across varying context lengths.

1. Introduction

Modern Transformer architectures typically model temporal structure through positional mechanisms such as rotary positional embeddings (RoPE) (Su et al., 2024), which propagate representations through norm-preserving rotations. While this preserves relative phase information, it does not model uncertainty growth, treating distant and recent states as equally reliable. As a result, high-frequency components are not explicitly attenuated with temporal distance, which may contribute to interference during long-range aggregation and reduced stability under long-context extrapolation.

We reformulate self-attention as a form of robust state estimation, where past tokens are aggregated using weights determined by their consistency under a shared dynamical prior. We formalize this by introducing a linear time-invariant (LTI) stochastic differential equation (SDE) that serves as a local propagation and uncertainty prior at each query position, yielding closed-form expressions for both

transported means and their predicted uncertainty as a function of temporal lag.

By treating queries and keys as noisy observations under this shared dynamical prior, we derive Robust Filter Attention (RFA). RFA propagates keys into the query frame and computes lag-dependent uncertainty via the Differential Lyapunov Equation (DLE), yielding a precision prior consistent with transport under the learned linear dynamics. This precision is used in residual-based Mahalanobis scoring, allowing the model to weight tokens by their consistency after dynamical propagation. Thus, RFA functions as a parallelized robust filter: the dynamics define a shared transport and uncertainty model, while token weights adapt online through precision-weighted residuals.

To ensure computational tractability, RFA imposes four structural constraints: (1) LTI dynamics for analytic state and uncertainty propagation; (2) an approximate anchor-conditioned factorization of the likelihood across source tokens, enabling $\mathcal{O}(N^2)$ scaling; (3) simultaneous diagonalizability, enabling analytic solution of the DLE and closed-form precision inversion; and (4) an isotropic formulation, preserving the computational and memory complexity of standard attention.

In the zero-noise and zero-decay limit, our formulation reduces to a purely rotational embedding consistent with RoPE, while ALiBi (Press et al., 2022) can be interpreted as approximating the short-time linear growth of uncertainty predicted by the DLE under Brownian diffusion.

Finally, we introduce Spectrally-Coupled RFA (SC-RFA), which partitions the frequency spectrum across heads and couples each head’s dissipation rate (μ) to its maximum rotation frequency (ω_{\max}). This coupling enforces an inverse relationship between spectral resolution and temporal persistence: high-frequency heads act as sharp, short-range filters, while low-frequency heads function as stable long-range integrators. This induces a multi-resolution prior that separates short- and long-range dependencies across heads.

Our contributions are:

- (i) Casting self-attention as approximate parallel robust state estimation under an SDE prior.
- (ii) A dynamical positional framework that recovers RoPE and ALiBi as limiting cases.

¹Independent Researcher, Los Angeles, CA, USA. Correspondence to: Peter Racioppo <pcracioppo@gmail.com>.

- (iii) A scalable isotropic formulation with analytic uncertainty propagation at standard attention cost.
- (iv) A spectrally coupled decay prior enabling multi-resolution temporal filtering.

2. Related Work

2.1. Probabilistic and Kernel Views of Attention

The standard Transformer architecture (Vaswani et al., 2017) computes attention scores via a scaled dot-product between queries and keys. While originally motivated by computational efficiency and the ability to capture long-range dependencies, a growing body of work has sought to interpret these weights as probabilities derived from latent statistical models.

Probabilistic Transformers (Gabbur et al., 2021) show that dot-product attention arises as a constrained limit of MAP inference in a Gaussian mixture model. The Bayesian Attention Mechanism (BAM) (Bianchessi et al., 2025) treats positional embeddings as explicit priors over token indices, while the Correlated Gaussian Process Transformer (CGPT) (Bui et al., 2024) interprets asymmetric projections through correlated Gaussian process inference. These approaches introduce probabilistic structure, but rely on static feature-space similarity or fixed prior covariances.

Other work has interpreted attention as a kernel regression estimator, modifying similarity geometry in feature space to improve robustness or variance properties (Tsai et al., 2019; Han et al., 2023; Nielsen et al., 2024; Liu et al., 2020; Goel & Bartlett, 2024).

RFA instead weights tokens by prediction error under a shared dynamical prior, with uncertainty evolving via the DLE. This yields a global weighted least-squares estimate of the latent state, rather than a mixture assignment or similarity-based kernel smoothing.

2.2. Filtering, Continuous Dynamics, and SSMs

Continuous-time sequence models often parameterize latent dynamics using Neural Ordinary Differential Equations (Neural ODEs) (Chen et al., 2018) and their stochastic extensions, Neural SDEs (Li et al., 2020; Shen & Cheng, 2025), which learn drift and diffusion functions from data. Several architectures integrate attention with continuous dynamics to handle irregular sampling or time-dependent relevance, including Continuous-Time Attention (Chien & Chen, 2021), Attentive Neural Processes (Kim et al., 2019), and ACE-NODE (Jhin et al., 2021). Self-Modulating Attention (SMA) (Chen et al., 2021) adjusts attention weights as a function of temporal distance.

Other work integrates neural networks with classical filter-

ing frameworks by learning components of the Kalman filter, such as gains, noise models, or update rules (Jahanshahi & Zhu, 2025; Revach et al., 2022; Liu et al., 2023; Wang et al., 2024; Cohen & Klein, 2025; Shen et al., 2025). In contrast, RFA assumes a structured linear SDE prior whose DLE admits a closed-form solution, enabling parallel precision-weighted aggregation without learning Kalman gains or full covariance updates.

State space models (SSMs) provide another approach to sequence modeling by assuming linear time-invariant (LTI) dynamics and converting recurrence into convolution via the state transition matrix $e^{\mathbf{A}\Delta t}$. Frameworks such as HiPPO (Gu et al., 2020) and S4 (Gu et al., 2022) achieve efficiency by restricting \mathbf{A} to diagonalizable or diagonal-plus-low-rank forms, reducing state propagation costs from $\mathcal{O}(d^2)$ to $\mathcal{O}(d)$. Recent work shows that causal linear attention can be viewed as a special case of LTI convolution (Dao & Gu, 2024).

Like S4 (Gu et al., 2022), RFA relies on diagonalizable linear dynamics for computational efficiency. However, whereas deterministic SSMs propagate only the state mean, RFA propagates second-order statistics via the DLE, yielding a time-dependent precision kernel that defines a prior over attention weights. While modern SSMs such as Mamba (Gu & Dao, 2024) achieve context sensitivity through data-dependent gating of the recurrent state, RFA preserves content-based routing through attention and regularizes it using a prior on predicted uncertainty.

2.3. Positional Encodings and Complex Geometry

Modeling relative temporal structure in Transformers has been approached with several geometric methods. RoPE (Su et al., 2024) encodes relative position as complex rotations of queries and keys, preserving phase relationships across time but introducing no explicit notion of decay or uncertainty. ALiBi (Press et al., 2022) instead applies a linear distance-based bias to attention logits, enforcing locality and improving length extrapolation by suppressing distant interactions. xPos (Sun et al., 2023b;a) generalizes RoPE by combining rotations with dimension-wise decay to stabilize long-range behavior.

While these methods impose useful geometric or monotonic structure, they are not derived from an explicit stochastic model of latent state evolution and do not specify how uncertainty should accumulate or dissipate over time. As a result, their decay and bias terms are typically introduced heuristically, rather than as consequences of a shared dynamical prior.

RFA performs value aggregation in the stationary eigenframe of the latent dynamics, necessitating a rotate-aggregate-rotate-back operation on the value stream.

This ensures that historical updates are aligned in a shared temporal frame before fusion, and then counter-rotated to remain equivariant with the observer’s evolving coordinate system. While methods such as RoPER (Harik, 2023) have applied value rotations previously, RFA derives this structure as the transformation required to maintain dynamical consistency of the state estimate under the shared latent dynamics.

Common positional embeddings can be viewed as limiting cases of a single latent stochastic process. RoPE implements deterministic phase transport without uncertainty accumulation, while ALiBi enforces locality via a distance bias consistent with a pure-diffusion prior. Similarly, xPos introduces dimension-wise decay but lacks an explicit model of uncertainty growth. By contrast, RFA derives both attenuation and reliability from an underlying SDE in which the same dissipation rate governs signal decay and uncertainty growth.

This unified parameterization ensures that temporal weighting and precision remain dynamically consistent rather than independently tuned. This distinguishes RFA from recent methods such as YaRN, CARoPE, and Selective RoPE (Peng et al., 2024; Veisi et al., 2025; Movahedi et al., 2025), which improve extrapolation through manual frequency scheduling or length-dependent scaling.

3. Methods

This section summarizes the formulation of RFA; complete derivations are provided in Appendix A and Appendix B.

3.1. Preliminaries

We model each token in a sequence of length N as a noisy observation of a latent linear time-invariant (LTI) stochastic dynamical system in state space $\mathbf{x}(t) \in \mathbb{R}^d$, observed at discrete times t_i as embeddings $\mathbf{z}_i \in \mathbb{R}^d$:

$$\begin{aligned} d\mathbf{x}(t) &= \mathbf{A} \mathbf{x}(t) dt + \mathbf{G} d\mathbf{w}(t), \\ \mathbf{z}_i &= \mathbf{C} \mathbf{x}(t_i) + \mathbf{v}(t_i), \end{aligned} \quad (1)$$

where $\mathbf{v}(t_i) \sim \mathcal{N}(\mathbf{0}, \mathbf{R})$ and $d\mathbf{w}(t)$ is a standard Wiener process.

We denote the latent output at time t_i by $\mathbf{z}_i^C := \mathbf{C}\mathbf{x}(t_i)$. Given a past measurement \mathbf{z}_j , we form a transported estimate of the latent output at time t_i by propagating through the dynamics:

$$\hat{\mathbf{z}}_{ij} := \Phi^C(\Delta t_{ij}) \mathbf{z}_j, \quad \Phi^C(\Delta t) := \mathbf{C} e^{\mathbf{A} \Delta t} \mathbf{C}^{-1},$$

where $\Delta t_{ij} = t_i - t_j$ and \mathbf{C} is assumed invertible.

Under the linear SDE, the transported estimate is distributed as:

$$\hat{\mathbf{z}}_{ij} \sim \mathcal{N}\left(\mathbf{z}_i^C, \mathbf{V}^C(\Delta t_{ij})\right),$$

where the covariance captures both accumulated process noise and the measurement noise of the source token:

$$\mathbf{V}^C(\Delta t) = \mathbf{C} \mathbf{V}(\Delta t) \mathbf{C}^\top + \Phi^C(\Delta t) \mathbf{R} \Phi^C(\Delta t)^\top.$$

Here, $\mathbf{V}(\Delta t)$ is the solution of the Differential Lyapunov Equation (DLE), which governs noise accumulation in linear SDEs:

$$\dot{\mathbf{V}}(s) = \mathbf{A} \mathbf{V}(s) + \mathbf{V}(s) \mathbf{A}^\top + \mathbf{Q}, \quad \mathbf{V}(0) = \mathbf{0}. \quad (2)$$

The anchor state is not observed directly. Instead, the model forms a query embedding:

$$\mathbf{z}_i = \mathbf{z}_i^C + \boldsymbol{\varepsilon}_\Gamma, \quad \boldsymbol{\varepsilon}_\Gamma \sim \mathcal{N}(\mathbf{0}, \mathbf{R}_\Gamma),$$

which is compared to transported past measurements $\hat{\mathbf{z}}_{ij}$. The observable residual is therefore:

$$\mathbf{r}_{ij} := \mathbf{z}_i - \hat{\mathbf{z}}_{ij}.$$

To obtain a parallelizable estimator, we approximate the joint likelihood by treating \mathbf{z}_i and $\hat{\mathbf{z}}_{ij}$ as conditionally independent noisy measurements of the same latent anchor state (see Appendix A.4). Under this approximation, the residual follows:

$$\mathbf{r}_{ij} \sim \mathcal{N}\left(\mathbf{0}, \mathbf{V}_{ij}^Z\right), \quad \mathbf{V}_{ij}^Z = \mathbf{V}_{ij}^C + \mathbf{R}_\Gamma.$$

where \mathbf{R}_Γ models irreducible uncertainty in the anchor representation and prevents precision from diverging as $\Delta t \rightarrow 0$. The corresponding precision is $\mathbf{P}_{ij}^Z := (\mathbf{V}_{ij}^Z)^{-1}$.

Relevance between a query and a key is measured by the squared Mahalanobis distance of the observable residual:

$$d_{ij}^2 = \mathbf{r}_{ij}^\top \mathbf{P}_{ij}^Z \mathbf{r}_{ij}, \quad (3)$$

which replaces dot-product similarity with a likelihood-based consistency test under the SDE prior.

We estimate the anchor state by minimizing the sum of squared Mahalanobis residuals over all transported observations:

$$\bar{\mathbf{z}}_i = \arg \min_{\mathbf{z}} \sum_{j \leq i} (\mathbf{z} - \hat{\mathbf{z}}_{ij})^\top \mathbf{P}_{ij}^Z (\mathbf{z} - \hat{\mathbf{z}}_{ij}).$$

Minimizing the resulting sum of independent negative log-likelihood terms yields the precision-weighted estimator:

$$\bar{\mathbf{z}}_i = \left(\sum_{j \leq i} \mathbf{P}_{ij}^Z \right)^{-1} \sum_{j \leq i} \mathbf{P}_{ij}^Z \hat{\mathbf{z}}_{ij}. \quad (4)$$

We obtain data-dependent weights by reweighting the prior precisions:

$$\mathbf{P}_{ij}^Z \rightarrow w_{ij} \mathbf{P}_{ij}^Z,$$

where w_{ij} is a scalar weight, whose functional form can be chosen according to the desired properties of the estimator:

$$w_{ij} \propto \begin{cases} \exp\left(-\frac{d_{ij}^2}{\nu}\right) & \text{(exponential kernel)} \\ \left(1 + \frac{d_{ij}^2}{\nu}\right)^{-\kappa} & \text{(power law)} \end{cases}$$

where ν is a scalar degrees-of-freedom parameter that governs the tail-weight of the estimator. For efficient implementation, we assume the dynamics are simultaneously diagonalizable by an invertible $\mathbf{S} \in \mathbb{C}^{d \times d}$. Under this assumption, the DLE decouples into scalar ODEs, yielding the closed-form solution:

$$\begin{aligned} \mathbf{V}(\Delta t_{ij}) &= \mathbf{S} \Lambda_{\mathbf{V}}(\Delta t_{ij}) \mathbf{S}^\dagger, \\ \Lambda_{\mathbf{V}}(\Delta t) &= \text{diag}\left(\lambda_{\mathbf{Q},k} \frac{1 - e^{2\text{Re}(\lambda_k) \Delta t}}{-2\text{Re}(\lambda_k)}\right). \end{aligned} \quad (5)$$

The total covariance in the eigenbasis is then:

$$\Lambda_{\mathbf{V}}^Z(\Delta t) = |\Lambda_{\mathbf{C}}|^2 \Lambda_{\mathbf{V}}(\Delta t) + e^{2\text{Re}(\Lambda) \Delta t} \Lambda_{\mathbf{R}} + \Lambda_{\Gamma},$$

where $\Lambda_{\mathbf{C}}, \Lambda_{\mathbf{R}}, \Lambda_{\Gamma}$ are the diagonalized output and noise matrices.

The Mahalanobis distance diagonalizes as:

$$d_{ij}^2 = \sum_{k=1}^d \lambda_{\mathbf{P},k}^Z(\Delta t_{ij}) |z_{s,k,i} - \hat{z}_{s,k,ij}|^2, \quad (6)$$

where $\mathbf{z}_s = \mathbf{S}^{-1} \mathbf{z}$ and $\hat{z}_{s,ij} = e^{\Lambda \Delta t_{ij}} z_{s,j}$.

The estimate in the eigenbasis then becomes:

$$\bar{z}_{s,i} = \sum_{j \leq i} \mathcal{A}_{ij} \odot \hat{z}_{s,ij}, \quad (7)$$

$$\mathcal{A}_{ij} := w_{ij} \lambda_{\mathbf{P},ij}^Z \odot \left(\sum_{j' \leq i} w_{ij'} \lambda_{\mathbf{P},ij'}^Z \right), \quad (8)$$

where $\lambda_{\mathbf{P}}^Z = \text{diag}(\Lambda_{\mathbf{P}}^Z)$, yielding head-wise, dimension-wise normalized attention weights.

3.2. Robust Filter Attention (RFA) Mechanism

We instantiate the robust state estimator as a complex-valued attention layer by identifying the abstract diagonalization matrices with learned linear projections. The input projections $\mathbf{W}_Q, \mathbf{W}_K, \mathbf{W}_V \in \mathbb{C}^{d \times d}$ learn the transformation into the SDE's decoupled eigenbasis, absorbing the inverse diagonalizing matrix \mathbf{S}^{-1} , while the output matrix \mathbf{W}_O absorbs \mathbf{S} , mapping the filtered estimates back to the original basis:

$$\mathbf{Q} = \mathbf{W}_Q \mathbf{Z}, \quad \mathbf{K} = \mathbf{W}_K \mathbf{Z}, \quad \mathbf{V} = \mathbf{W}_V \mathbf{Z} \in \mathbb{C}^{d \times N}.$$

To preserve the $\mathcal{O}(N^2 + Nd)$ memory complexity of standard attention, we impose isotropic decay and noise in the learned eigenbasis (per head):

$$\Lambda = -\mu \mathbf{I} + i\Lambda_{\Omega}, \quad \Lambda_{\mathbf{Q}} = \sigma^2 \mathbf{I}, \quad \Lambda_{\mathbf{R}} = \eta^2 \mathbf{I}, \quad \Lambda_{\Gamma} = \gamma^2 \mathbf{I}.$$

where $\omega_k \in \mathbb{R}$, $\mu, \sigma^2, \eta^2, \gamma^2 \in \mathbb{R}^+$, and $\Lambda_{\Omega} \in \mathbb{R}^{d \times d}$ is diagonal. These definitions ensure (marginally) stable dynamics and positive semi-definite noise covariances.

Under isotropic decay and noise, each eigenmode follows independent exponentially decaying rotations with decay μ and angular frequency ω_k . This yields simple element-wise rotation factors for forward/backward propagation, and a decay kernel that depends only on the time lag Δt_{ij} :

$$\tilde{\Phi}^-[k, i] = e^{-i\omega_k t_i}, \quad \tilde{\Phi}^+[k, i] = e^{i\omega_k t_i}, \quad \mathbf{E}[i, j] = e^{-\mu \Delta t_{ij}}.$$

We define rotated queries, keys, and values:

$$\tilde{\mathbf{Q}} = \tilde{\Phi}^- \odot \mathbf{Q}, \quad \tilde{\mathbf{K}} = \tilde{\Phi}^- \odot \mathbf{K}, \quad \tilde{\mathbf{V}} = \tilde{\Phi}^- \odot \mathbf{V}.$$

The isotropic constraints cause the variance to become independent of the feature dimension:

$$\mathbf{V}_{\Delta t}[i, j] := \tilde{\sigma}^2 (1 - e^{-2\mu \Delta t_{ij}}) + \eta^2 e^{-2\mu \Delta t_{ij}} + \gamma^2 \quad (9)$$

Here, $\tilde{\sigma}^2 := \frac{\lambda_{\mathbf{Q}}^2 \sigma^2}{2\mu}$, η^2 , and γ^2 are learned scalar parameters (per head), corresponding respectively to steady-state process uncertainty, historical measurement noise (key-side), and anchor-point uncertainty at the reference timestep (query-side).

This allows the Mahalanobis distance for all pairs (i, j) to be computed by element-wise multiplying a matrix of scalar precisions $\mathbf{P}_{\Delta t}[i, j] := 1/\mathbf{V}_{\Delta t}[i, j]$ by the scalar squared residual norms $\|\mathbf{R}_{qk}[i, j]\|^2$:

$$\mathbf{D}^2[i, j] = \mathbf{P}_{\Delta t}[i, j] \cdot \|\mathbf{R}_{qk}[i, j]\|^2.$$

where the ij th residual is:

$$\mathbf{R}_{qk}[i, j] := \tilde{\mathbf{Q}}_i - \mathbf{E}[i, j] \cdot \tilde{\mathbf{K}}_j.$$

The squared residual norm decomposes into a query magnitude term, a decayed key magnitude term, and a cross-term containing the complex inner product:

$$\begin{aligned} \|\mathbf{R}_{qk}[i, j]\|^2 &= \|\mathbf{Q}_i\|^2 + \mathbf{E}[i, j]^2 \|\mathbf{K}_j\|^2 \\ &\quad - 2 \mathbf{E}[i, j] \text{Re}(\tilde{\mathbf{Q}}_i^\dagger \tilde{\mathbf{K}}_j). \end{aligned} \quad (10)$$

where $*$ denotes the complex conjugate.

We use a Student's t attention logit, which improves robustness to outliers:

$$\mathbf{L} = \log(\mathbf{P}_{\Delta t}) - \kappa \log \left(1 + \frac{1}{\nu} \mathbf{P}_{\Delta t} \odot \|\mathbf{R}_{qk}\|^2 \right), \quad (11)$$

where $\kappa := \frac{\nu+d}{d}$. The attention matrix is then $\mathbf{A} = \hat{\mathbf{A}} \odot \mathbf{E}$, where:

$$\hat{\mathbf{A}} = \text{Softmax}_j(\mathbf{L} + \mathbf{M}_{\text{causal}}),$$

where $\mathbf{M}_{\text{causal}}$ is a causal mask.

The filtered estimate $\bar{\mathbf{Z}}$ is computed by aggregating the rotated values, rotating the values back into the value frame, and projecting back to the original basis:

$$\bar{\mathbf{V}} = \tilde{\Phi}^+ \odot (\tilde{\mathbf{V}} \mathbf{A}^\top), \quad \bar{\mathbf{Z}} = \mathbf{W}_O \bar{\mathbf{V}}.$$

RFA's complex-valued operations can be represented entirely in the real domain, as detailed in Appendix D.1. The complete implementation of the Isotropic RFA mechanism is formalized in Algorithm 1 in Appendix D.3.¹

3.3. Dynamical Self-Consistency and Positional Embeddings

In RFA, the same decay rate μ governs both signal attenuation under state propagation and the evolution of the precision prior $\mathbf{P}_{\Delta t}$. This enforces dynamical self-consistency between how past states are transported and how their reliability is assessed.

RFA employs a rotate–aggregate–rotate-back structure on the value stream. Values are first mapped into a shared reference frame using $\tilde{\Phi}^-$, aggregated in that frame, and then transported back to the query frame via $\tilde{\Phi}^+$. This alignment is required for the aggregation to correspond to a valid fusion of latent state estimates under the shared dynamical model; without it, values would be combined in mismatched temporal coordinates, breaking the interpretation of the update as a coherent state estimate.

Several common positional embeddings arise as limiting cases of this formulation (see Appendix B.4). In the deterministic zero-decay limit ($\mu = 0, \sigma^2 = 0$), state evolution reduces to pure rotations, recovering the geometry of Rotary Positional Embeddings (RoPE). In the zero-decay, small-lag regime, the logarithm of the DLE-predicted precision yields an approximately linear distance penalty, recovering the additive bias structure of ALiBi.

The relative magnitudes of measurement noise (η^2) and steady-state process uncertainty ($\tilde{\sigma}^2$) determine the effective filtering regime of each head. Heads may specialize into an **integrative regime**, where early measurements are unreliable and precision increases after short lags as the latent state stabilizes, or a **diffusive regime**, where recent observations dominate and uncertainty progressively suppresses distant history. This allows different heads to specialize in distinct filtering regimes under the same attention expression.

¹A multi-head implementation is available at <https://github.com/PCR-git/Robust-Filter-Attention>.

3.4. Spectrally Coupled Dynamics (SC-RFA)

Standard positional mechanisms such as RoPE employ a fixed frequency bank across all heads, allowing high-frequency oscillations to persist indefinitely. At long horizons, this leads to spectral aliasing, where the lack of attenuation makes it difficult to distinguish between fast and slow dynamics.

To address this, we introduce Spectrally Coupled RFA (SC-RFA), which enforces a frequency-dependent dissipation prior: higher frequencies should decay more rapidly. We partition a global frequency bank Ω monotonically across heads, assigning each head h a spectral band $[\omega_{h,\min}, \omega_{h,\max}]$, and couple the dissipation rate in each head to its maximum frequency:

$$\mu_h = b \cdot \omega_{h,\max},$$

where $b \in \mathbb{R}^+$ is a shared damping ratio.

This coupling imposes an inverse relationship between spectral resolution and temporal persistence. High-frequency heads act as sharp, short-range filters, while low-frequency heads behave as stable long-range integrators. The resulting multi-resolution prior stabilizes long-range phase behavior while preserving local expressiveness.

4. Experimental Evaluation and Ablations

We evaluate whether explicitly modeling uncertainty growth improves long-context stability while preserving short-range accuracy, comparing RFA against two widely used positional baselines derived from deterministic geometry (RoPE) (Su et al., 2024) and monotonic biasing (ALiBi) (Press et al., 2022), respectively.

4.1. Experimental Setup

Architecture: All models use a 6-layer Transformer with $h = 8$ heads and embedding dimension $d = 256$. To ensure comparable model capacity, we apply identical $d \rightarrow 2d \rightarrow d$ projections in both RFA and the RoPE/ALiBi baselines. RFA introduces only a small number of additional scalar parameters per head for noise and robustness, increasing total parameter count by approximately 0.02%. We employ a pre-norm architecture with an FFN expansion factor of 4. Models are trained for 15 epochs using Adam with a cosine learning rate schedule.

Datasets. We evaluate on WikiText-103, a large-scale word-level language modeling benchmark derived from Wikipedia articles and used to measure perplexity and long-context extrapolation (Merity et al., 2017), and on BabyLM-2025 (Strict), a curated English language modeling corpus used as a complementary benchmark under the same training and evaluation protocol (Charpentier et al., 2025).

Table 1. Long-context extrapolation on WikiText-103 (Test PPL). All models were trained with a fixed context window of 512 tokens.

Model	L=512	L=1024	L=2048	L=4096
RoPE (B1)	28.48	30.94	44.21	72.69
ALiBi (B2)	28.59	27.30	26.54	26.30
Decayed RoPE (B3)	28.52	29.42	34.68	44.00
SC-RoPE (B4)	28.36	29.02	34.99	44.17
RFA (M1)	28.01	27.58	29.99	38.46
SC-RFA (M2)	27.54	26.73	29.46	37.19
<i>Structural Ablations (Relative to M2)</i>				
Gaussian NLL (M2.1)	27.98	27.16	28.95	33.51
Flat Prior (M2.2)	27.69	28.71	38.11	62.83
No Mult. Gate (M2.3)	27.65	29.01	39.18	57.30
No Value Rot. (M2.4)	30.24	92.08	187.29	463.29
No Rotations (M2.5)	28.58	27.25	26.61	26.83
Pure Rotation (M2.6)	27.97	35.59	69.39	131.29

Full architectural details and detailed descriptions of all model variants are provided in Appendix E. Analysis of attention maps and noise parameters are provided in Appendix F.

4.2. Results on Wikitext-103

We evaluate extrapolation by measuring test perplexity on WikiText-103 at increasing context lengths $L \in \{512, 1024, 2048, 4096\}$, after training all models with a fixed context window of 512 tokens. We compare against standard positional baselines (RoPE, ALiBi), and include two geometry-only decay variants to isolate the effect of damping in rotational embeddings: Decayed RoPE (B3), which applies exponential decay with distance, as in RFA, and SC-RoPE (B4), which couples decay rates to head-wise frequency bands as in SC-RFA. These baselines test whether decay and spectral coupling alone can explain extrapolation gains, without modeling uncertainty.

We evaluate RFA (M1) and SC-RFA (M2), along with structural ablations relative to M2, designed to isolate the effect of its components when removed: the robust weight (M2.1); the DLE-derived precision prior (M2.2); the multiplicative gating term (M2.3); value rotations (M2.4); all rotations (M2.5); finally, we test a purely rotational, zero dissipation and noise noise variant, analogous to RoPER (M2.6). Results are shown in Table 1.

RFA variants achieve both stronger local performance and improved extrapolation relative to RoPE. In particular, SC-RFA (M2) improves over RoPE by 0.94 PPL at $L = 512$ and reduces degradation at long horizons, reaching 37.19 PPL at $L = 4096$ compared to RoPE’s 72.69. This behavior emerges under a fixed training protocol without requiring length-dependent scaling rules or curriculum schedules.

Introducing decay into rotational embeddings (B3) and spectrally coupling decay across heads (B4) slows the long-range degradation of RoPE. However, both geometry-only variants under-perform RFA across all context lengths, indicating that decay alone is insufficient without explicit uncertainty modeling.

Compared to ALiBi, SC-RFA achieves lower perplexity at the training length ($L = 512$) and at moderate extrapolation ($L = 1024$), suggesting improved utilization of fine-grained temporal structure when uncertainty remains bounded. At longer horizons, ALiBi attains lower perplexity by enforcing strong locality, while SC-RFA continues to integrate distant context with attenuated but nonzero precision. This reflects a trade-off between aggressive locality and uncertainty-weighted long-range integration.

The non-robust variant (M2.1) exhibits a different trade-off: it under-performs the robust estimator at the training horizon, but achieves lower perplexity at extreme extrapolation lengths. This is consistent with Gaussian likelihoods imposing stronger quadratic penalties on residuals, which suppress extreme deviations more aggressively but reduce sensitivity to small errors when uncertainty is low.

Removing the DLE-derived precision prior (M2.2) leads to degradation at long horizons, with perplexity increasing to 62.83 at $L = 4096$, indicating that representing uncertainty is necessary to control the influence of distant tokens. Removing the multiplicative gating term (M2.3) causes degradation within the training window and worsens extrapolation, suggesting that both the additive and multiplicative precision terms contribute to stability.

Eliminating value-space rotation and counter-rotation (M2.4) causes severe degradation at long context, reaching 463.29 PPL at $L = 4096$. This is consistent with aggregation no longer corresponding to fusion of latent state estimates in a shared temporal frame. Removing all rotations (M2.5) degrades short-context performance but yields strong long-range stability.

In the zero-noise, zero-decay, pure rotational limit (M2.6), perplexity increases sharply with context length, reflecting the accumulation of unattenuated high-frequency components from distant tokens. This supports the necessity of dissipation to prevent long-range spectral interference in rotational attention mechanisms.

Table 2 analyzes the effect of the damping coefficient b in SC-RFA. Smaller values of b yield slower decay, improving short-context performance but leading to faster degradation as context increases. Larger values of b produce stronger attenuation and more stable long-range behavior at the cost of reduced short-range precision. Notably, for sufficiently strong damping (e.g., $b = 5 \times 10^{-1}$), SC-RFA outperforms ALiBi at intermediate horizons ($L = 2048$), with ALiBi

Table 2. Sensitivity Analysis of the Damping Coefficient b in SC-RFA (M2). Results show Test PPL on WikiText-103 across increasing context lengths.

Damping (b)	L=512	L=1024	L=2048	L=4096
5×10^{-4}	27.60	28.88	37.34	51.48
5×10^{-3}	27.60	28.71	35.35	43.90
5×10^{-2}	27.54	26.73	29.46	37.19
5×10^{-1}	27.61	26.38	26.37	29.72
5×10^0	27.91	26.68	26.37	28.16

Table 3. Long-context extrapolation on BabyLM-2025 (Test PPL). All models were trained with a fixed context window of 512 tokens.

Model	L=512	L=1024	L=2048	L=4096
RoPE (B1)	17.70	18.78	23.33	33.29
ALiBi (B2)	17.70	17.20	17.06	17.51
RFA (M1)	17.51	17.71	20.61	31.04
SC-RFA (M2)	17.36	16.99	18.33	22.25

retaining an advantage only at the largest tested context length. This behavior is consistent with b acting as a global timescale parameter that controls how rapidly past information is discounted, yielding a predictable stability–resolution trade-off.

4.3. Results on BabyLM-2025

We use the same architectures, hyperparameters, and training protocol as on WikiText-103.

On BabyLM-2025, where language modeling performance is more strongly dominated by short-range context, differences between positional mechanisms are smaller at short context lengths. Both RFA variants outperform RoPE at all evaluated context lengths and outperform ALiBi within the training window. SC-RFA also achieves lower perplexity than ALiBi at intermediate context ($L = 1024$), while ALiBi remains strongest at the largest horizons due to its strict locality bias. Overall, these results mirror the trade-off observed on WikiText-103: uncertainty-aware precision weighting improves robustness over purely rotational embeddings while retaining stronger short- and mid-range performance than aggressively local positional biases.

4.4. Learning Dynamics and Head Specialization

RFA variants converge faster and achieve lower validation perplexity earlier in training than RoPE and ALiBi, indicating that the SDE-based prior provides an effective inductive bias for latent state estimation (Appendix F.1). Analysis of learned noise, decay, and robustness parameters reveals systematic head specialization into distinct uncertainty and selectivity regimes, with different heads converging to dif-

ferent tolerances for temporal inconsistency and noise (Appendix F.2).

Attention map visualizations at long context lengths further reveal an emergent integrative regime in low-decay heads, where recent tokens are initially downweighted and historical states receive increasing emphasis as uncertainty stabilizes (Appendix F). Spectral coupling in SC-RFA substantially alters long-range attention structure: compared to RFA and RoPE, heads exhibit fewer and sharper periodic bands, reduced checkerboard aliasing, and clearer separation between local and long-range interactions (Appendix F). Together, these diagnostics support the interpretation of RFA as learning uncertainty-aware temporal filtering rather than relying solely on geometric positional bias.

5. Conclusion

We show that self-attention can be reformulated as a tractable precision-weighted state estimator under a linear time-invariant SDE prior. This yields Robust Filter Attention (RFA), a dynamically consistent and uncertainty-aware generalization of standard attention. RFA preserves the asymptotic complexity of standard attention while propagating uncertainty through linear dynamics and performing robust Mahalanobis reweighting, improving both in-window performance and long-context stability. We show that rotary and linear bias positional embeddings can be recovered as limiting cases of this filtering formulation. We also introduce SC-RFA, which enforces frequency-dependent dissipation and further improves performance by separating short- and long-range temporal structure across heads.

Future work should examine whether RFA’s simplifying assumptions—such as isotropic noise and simultaneously diagonalizable dynamics—can be relaxed while maintaining computational tractability. Another promising direction is to characterize the relationship between filtering-based formulations of attention and recurrent state-space models, and to study how these perspectives interact with normalization, residual connections, and depth in Transformers.

Impact Statement

This work provides a method for uncertainty propagation in attention-based models. We do not identify any ethical concerns beyond those generally associated with advances in machine learning methodology.

References

Bianchessi, A. S., Aguirre, Y. C., Barros, R. C., and Kupssinskü, L. S. Bayesian attention mechanism: A probabilistic framework for positional encoding and context length extrapolation, 2025. URL <https://arxiv.org/abs/2501.01234>.

org/abs/2505.22842.

Bui, L. M., Huu, T. T., Dinh, D., Nguyen, T. M., and Hoang, T. N. Revisiting kernel attention with correlated Gaussian process representation. In *Proceedings of the Fortieth Conference on Uncertainty in Artificial Intelligence*, UAI '24. JMLR.org, 2024.

Charpentier, L., Choshen, L., Cotterell, R., Gul, M. O., Hu, M. Y., Liu, J., Jumelet, J., Linzen, T., Mueller, A., Ross, C., Shah, R. S., Warstadt, A., Wilcox, E. G., and Williams, A. Findings of the third BabyLM challenge: Accelerating language modeling research with cognitively plausible data. In Charpentier, L., Choshen, L., Cotterell, R., Gul, M. O., Hu, M. Y., Liu, J., Jumelet, J., Linzen, T., Mueller, A., Ross, C., Shah, R. S., Warstadt, A., Wilcox, E. G., and Williams, A. (eds.), *Proceedings of the First BabyLM Workshop*, pp. 399–420, Suzhou, China, November 2025. Association for Computational Linguistics. doi: 10.18653/v1/2025.babylm-main.28. URL <https://aclanthology.org/2025.babylm-main.28/>.

Chen, C., Geng, H., Yang, N., Yan, J., Xue, D., Yu, J., and Yang, X. Learning self-modulating attention in continuous time space with applications to sequential recommendation. In Meila, M. and Zhang, T. (eds.), *Proceedings of the 38th International Conference on Machine Learning*, volume 139 of *Proceedings of Machine Learning Research*, pp. 1606–1616. PMLR, 18–24 Jul 2021. URL <https://proceedings.mlr.press/v139/chen21h.html>.

Chen, R. T. Q., Rubanova, Y., Bettencourt, J., and Duvenaud, D. Neural ordinary differential equations. In *Proceedings of the 32nd International Conference on Neural Information Processing Systems*, NIPS'18, pp. 6572–6583, Red Hook, NY, USA, 2018. Curran Associates Inc.

Chien, J.-T. and Chen, Y.-H. Continuous-time self-attention in neural differential equation. In *ICASSP 2021 - 2021 IEEE International Conference on Acoustics, Speech and Signal Processing (ICASSP)*, pp. 3290–3294, 2021. doi: 10.1109/ICASSP39728.2021.9414104.

Cohen, N. and Klein, I. Adaptive Kalman-informed Transformer. *Engineering Applications of Artificial Intelligence*, 146:110221, April 2025. ISSN 0952-1976. doi: 10.1016/j.engappai.2025.110221. URL <http://dx.doi.org/10.1016/j.engappai.2025.110221>.

Dao, T. and Gu, A. Transformers are SSMs: generalized models and efficient algorithms through structured state space duality. In *Proceedings of the 41st International Conference on Machine Learning*, ICML'24. JMLR.org, 2024.

Gabbur, P., Bilkhu, M., and Movellan, J. Probabilistic attention for interactive segmentation. In Beygelzimer, A., Dauphin, Y., Liang, P., and Vaughan, J. W. (eds.), *Advances in Neural Information Processing Systems*, 2021. URL <https://openreview.net/forum?id=JpD1WGTBHB>.

Goel, G. and Bartlett, P. Can a Transformer represent a Kalman filter? In Abate, A., Cannon, M., Margellos, K., and Papachristodoulou, A. (eds.), *Proceedings of the 6th Annual Learning for Dynamics & Control Conference*, volume 242 of *Proceedings of Machine Learning Research*, pp. 1502–1512. PMLR, 15–17 Jul 2024. URL <https://proceedings.mlr.press/v242/goel24a.html>.

Gu, A. and Dao, T. Mamba: Linear-time sequence modeling with selective state spaces. In *First Conference on Language Modeling*, 2024. URL <https://openreview.net/forum?id=tEYskw1VY2>.

Gu, A., Dao, T., Ermon, S., Rudra, A., and Ré, C. HiPPO: recurrent memory with optimal polynomial projections. In *Proceedings of the 34th International Conference on Neural Information Processing Systems*, NIPS '20, Red Hook, NY, USA, 2020. Curran Associates Inc. ISBN 9781713829546.

Gu, A., Goel, K., and Re, C. Efficiently modeling long sequences with structured state spaces. In *International Conference on Learning Representations*, 2022. URL <https://openreview.net/forum?id=uYLFoz1vlAC>.

Han, X., Ren, T., Nguyen, T. M., Nguyen, K., Ghosh, J., and Ho, N. Designing robust Transformers using robust kernel density estimation. In *Thirty-seventh Conference on Neural Information Processing Systems*, 2023. URL <https://openreview.net/forum?id=BqTvlMtuhu>.

Harik, G. Rotary positional embeddings with relative distance (RoPER). <https://research.labml.ai/RoPER.html>, 2023. Online implementation and derivation via labml.ai.

Jahanshahi, H. and Zhu, Z. H. Uncertainty propagation networks for neural ordinary differential equations, 2025. URL <https://arxiv.org/abs/2508.16815>.

Jhin, S. Y., Jo, M., Kong, T., Jeon, J., and Park, N. ACE-NODE: Attentive co-evolving neural ordinary differential equations. In *Proceedings of the 27th ACM SIGKDD Conference on Knowledge Discovery & Data Mining*, KDD '21, pp. 736–745, New York, NY, USA, 2021. Association for Computing Machinery. ISBN 9781450383325. doi: 10.1145/3447548.3467419. URL <https://doi.org/10.1145/3447548.3467419>.

Kim, H., Mnih, A., Schwarz, J., Garnelo, M., Eslami, A., Rosenbaum, D., Vinyals, O., and Teh, Y. W. Attentive neural processes. In *International Conference on Learning Representations*, 2019. URL <https://openreview.net/forum?id=Ske6PjC9KX>.

Li, X., Wong, T.-K. L., Chen, R. T. Q., and Duvenaud, D. K. Scalable gradients and variational inference for stochastic differential equations. In Zhang, C., Ruiz, F., Bui, T., Dieng, A. B., and Liang, D. (eds.), *Proceedings of The 2nd Symposium on Advances in Approximate Bayesian Inference*, volume 118 of *Proceedings of Machine Learning Research*, pp. 1–28. PMLR, 08 Dec 2020. URL <https://proceedings.mlr.press/v118/li20a.html>.

Liu, H., Lu, J., Zhao, X., Xu, S., Peng, H., Liu, Y., Zhang, Z., Li, J., Jin, J., Bao, Y., and Yan, W. Kalman filtering attention for user behavior modeling in CTR prediction. In *Proceedings of the 34th International Conference on Neural Information Processing Systems*, NIPS ’20, Red Hook, NY, USA, 2020. Curran Associates Inc. ISBN 9781713829546.

Liu, W., Lai, Z., Bacsa, K., and Chatzi, E. Neural extended Kalman filters for learning and predicting dynamics of structural systems. *Structural Health Monitoring*, 23(2): 1037–1052, June 2023. ISSN 1741-3168. doi: 10.1177/14759217231179912. URL <http://dx.doi.org/10.1177/14759217231179912>.

Merity, S., Xiong, C., Bradbury, J., and Socher, R. Pointer sentinel mixture models. In *International Conference on Learning Representations*, 2017. URL <https://openreview.net/forum?id=Byj72udxe>.

Movahedi, S., Carstensen, T., Afzal, A., Hutter, F., Orvieto, A., and Cevher, V. Selective rotary position embedding. *CoRR*, abs/2511.17388, November 2025. URL <https://doi.org/10.48550/arXiv.2511.17388>.

Nielsen, S., Abdullaev, L., Teo, R., and Nguyen, T. M. Elliptical attention. In *The Thirty-eighth Annual Conference on Neural Information Processing Systems*, 2024. URL <https://openreview.net/forum?id=Ejg4d4FVrs>.

Peng, B., Quesnelle, J., Fan, H., and Shippole, E. YaRN: Efficient context window extension of large language models. In *The Twelfth International Conference on Learning Representations*, 2024. URL <https://openreview.net/forum?id=wHBfxhZulu>.

Press, O., Smith, N., and Lewis, M. Train short, test long: Attention with linear biases enables input length extrapolation. In *International Conference on Learning Representations*, 2022. URL <https://openreview.net/forum?id=R8sQPpGCv0>.

Revach, G., Shlezinger, N., Ni, X., Escoriza, A. L., van Sloun, R. J. G., and Eldar, Y. C. KalmanNet: Neural network aided Kalman filtering for partially known dynamics. *IEEE Transactions on Signal Processing*, 70: 1532–1547, 2022. ISSN 1941-0476. doi: 10.1109/tsp.2022.3158588. URL <http://dx.doi.org/10.1109/TSP.2022.3158588>.

Shen, M. and Cheng, C. Neural SDEs as a unified approach to continuous-domain sequence modeling, 2025. URL <https://arxiv.org/abs/2501.18871>.

Shen, S., Chen, J., Yu, G., Zhai, Z., and Han, P. KalmanFormer: using Transformer to model the Kalman gain in Kalman filters. *Frontiers in Neurorobotics*, 18:1460255, 2025. doi: 10.3389/fnbot.2024.1460255. URL <https://doi.org/10.3389/fnbot.2024.1460255>.

Su, J., Ahmed, M., Lu, Y., Pan, S., Bo, W., and Liu, Y. RoFormer: Enhanced transformer with rotary position embedding. *Neurocomput.*, 568(C), February 2024. ISSN 0925-2312. doi: 10.1016/j.neucom.2023.127063. URL <https://doi.org/10.1016/j.neucom.2023.127063>.

Sun, Y., Dong, L., Huang, S., Ma, S., Xia, Y., Xue, J., Wang, J., and Wei, F. Retentive Network: A successor to Transformer for large language models, 2023a. URL <https://arxiv.org/abs/2307.08621>.

Sun, Y., Dong, L., Patra, B., Ma, S., Huang, S., Benhaim, A., Chaudhary, V., Song, X., and Wei, F. A length-extrapolatable Transformer. In Rogers, A., Boyd-Graber, J., and Okazaki, N. (eds.), *Proceedings of the 61st Annual Meeting of the Association for Computational Linguistics (Volume 1: Long Papers)*, pp. 14590–14604, Toronto, Canada, July 2023b. Association for Computational Linguistics. doi: 10.18653/v1/2023.acl-long.816. URL <https://aclanthology.org/2023.acl-long.816>.

Tsai, Y.-H. H., Bai, S., Yamada, M., Morency, L.-P., and Salakhutdinov, R. Transformer dissection: A unified understanding for Transformer’s attention via the lens of kernel. In Inui, K., Jiang, J., Ng, V., and Wan, X. (eds.), *Proceedings of the 2019 Conference on Empirical Methods in Natural Language Processing and the 9th International Joint Conference on Natural Language Processing (EMNLP-IJCNLP)*, pp. 4344–4353, Hong Kong, China, November 2019. Association for Computational Linguistics. doi: 10.18653/v1/D19-1443. URL <https://aclanthology.org/D19-1443>.

Vaswani, A., Shazeer, N., Parmar, N., Uszkoreit, J., Jones, L., Gomez, A. N., Kaiser, L. u., and Polosukhin, I. Attention is all you need. In Guyon, I., Luxburg, U. V., Bengio, S., Wallach, H., Fergus, R., Vishwanathan, S.,

and Garnett, R. (eds.), *Advances in Neural Information Processing Systems*, volume 30. Curran Associates, Inc., 2017. URL https://proceedings.neurips.cc/paper_files/paper/2017/file/3f5ee243547dee91fb053c1c4a845aa-Paper.pdf.

Veisi, A., Fartoot, D., and Amirzadeh, H. Context-aware rotary position embedding, 2025. URL <https://arxiv.org/abs/2507.23083>.

Wang, J., Geng, X., and Xu, J. Nonlinear Kalman filtering based on self-attention mechanism and lattice trajectory piecewise linear approximation, 2024. URL <https://arxiv.org/abs/2404.03915>.

Appendix Table of Contents

1. Appendix A: Attention as Parallelized Robust State Estimation	12
• <i>Derives self-attention as parallel robust state estimation under a linear SDE prior with analytically propagated uncertainty.</i>	
2. Appendix B: Robust Filter Attention Mechanism	19
• <i>Derives the transition from the full anisotropic tensor formulation of RFA to the scalable isotropic variant. Also provides a physical interpretation of common positional embeddings, showing how RoPE and ALiBi arise as limiting cases of the RFA framework.</i>	
3. Appendix C: Model Extensions	26
• <i>Describes extensions including Spectrally-Coupled RFA, inhomogeneous drift, and a confidence-based information fusion gate.</i>	
4. Appendix D: Implementation Details	31
• <i>Provides the complex-to-real isomorphism for hardware-efficient computation and full pseudocode for the isotropic RFA layer.</i>	
5. Appendix E: Experimental Details and Ablations	34
• <i>Defines all ablation variants, training setup, and hyperparameters.</i>	
6. Appendix F: Additional Experimental Results	36
• <i>Analyzes learned noise parameters, head specialization, and long-context attention maps to illustrate how RFA implements multi-scale filtering behavior in practice.</i>	

A. Attention as Parallel State Estimation.

We interpret attention as a parallel state estimation procedure under a shared linear dynamical prior. Rather than defining a single global generative model for the entire sequence, the SDE acts as a local prior at each anchor position: it specifies how other tokens are transported to that anchor time and how uncertainty grows with temporal separation. Under this view, each token provides a noisy, dynamically transported prediction of the anchor state, and attention aggregates these predictions in a precision-weighted manner.

We first review how uncertainty propagates under a linear SDE. We then show how this yields a pairwise consistency score between tokens based on predicted residual variance. Next, we derive attention as a parallel precision-weighted estimator of the anchor state under a conditional independence approximation. Finally, we apply robust M-estimation to obtain data-dependent reweighting of these precision terms.

A.1. Propagation of Uncertainty Through a Linear SDE

We consider a linear time-invariant Itô SDE as a shared prior over latent representations, used to define how uncertainty and similarity propagate across time, with latent state $\mathbf{x}(t)$ and observations \mathbf{z}_i :

$$d\mathbf{x}(t) = \mathbf{A}\mathbf{x}(t) dt + \mathbf{G}dw(t), \quad \mathbf{z}_i = \mathbf{C}\mathbf{x}(t_i) + \mathbf{v}(t_i),$$

where $dw(t)$ is standard Wiener noise, $\mathbf{v}(t_i)$ is measurement noise, and \mathbf{C} is assumed to be invertible. Our aim is to estimate the latent trajectory $\{\mathbf{x}_i\}_{i=1}^N$ from the sequence of noisy measurements $\{\mathbf{z}_j\}_{j=1}^N$. Since \mathbf{C} is invertible, this is equivalent to estimating $\mathbf{z}_i^C := \mathbf{C}\mathbf{x}(t_i)$, and we work in this space for convenience.

A.1.1. STATE PROPAGATION AND COVARIANCE ACCUMULATION

For a past measurement at t_j and a target time t_i , letting $\Delta t_{ij} = t_i - t_j$, the conditional mean at time t_i given $\mathbf{x}(t_j)$ under the linear dynamics is:

$$\hat{\mathbf{x}}_{ij} = e^{\mathbf{A}\Delta t_{ij}}\mathbf{x}(t_j).$$

This defines how a past latent state is transported into the reference frame of time t_i under the shared dynamics. The accumulated process noise over Δt_{ij} is given by the state covariance:

$$\mathbf{V}(\Delta t_{ij}) = \int_0^{\Delta t_{ij}} e^{\mathbf{A}s} \mathbf{Q} e^{\mathbf{A}^\top s} ds, \quad \mathbf{Q} = \mathbf{G}\mathbf{G}^\top,$$

which satisfies the differential Lyapunov equation (DLE):

$$\frac{d}{ds} \mathbf{V}(s) = \mathbf{A}\mathbf{V}(s) + \mathbf{V}(s)\mathbf{A}^\top + \mathbf{Q}, \quad \mathbf{V}(0) = 0.$$

The propagated state is Gaussian:

$$\hat{\mathbf{x}}_{ij} \sim \mathcal{N}(\mathbf{x}(t_i), \mathbf{V}(\Delta t_{ij})).$$

Thus, the uncertainty of the conditional mean grows or contracts with temporal separation depending on the values of \mathbf{A} and \mathbf{Q} . Backward propagation from a future measurement ($t_j > t_i$, i.e. the non-causal case) may be defined analogously via:

$$\mathbf{V}_B(\Delta t_{ij}) = e^{\mathbf{A}\Delta t_{ij}} \mathbf{V}(|\Delta t_{ij}|) e^{\mathbf{A}^\top \Delta t_{ij}},$$

yielding the same Gaussian form with covariance $\mathbf{V}_B(\Delta t_{ij})$.

A.1.2. MEASUREMENT COVARIANCE AND PRECISION

RFA requires the estimate of the current measurement $\mathbf{z}_i^C = \mathbf{C}\mathbf{x}(t_i)$ given a past measurement \mathbf{z}_j . We define a ‘pulled-forward’ (conditional mean) measurement as:

$$\hat{\mathbf{z}}_{ij} = \Phi^C(\Delta t_{ij}) \mathbf{z}_j, \quad \Phi^C(\Delta t_{ij}) = \mathbf{C} e^{\mathbf{A}\Delta t_{ij}} \mathbf{C}^{-1}.$$

This represents how a past observed token is mapped into the coordinate system of the target time step before comparison or aggregation.

The total propagated measurement covariance combines (i) accumulated process noise between t_j and t_i , and (ii) the measurement noise of the source token propagated through the dynamics:

$$\mathbf{V}^C(\Delta t_{ij}) = \mathbf{C} \mathbf{V}(\Delta t_{ij}) \mathbf{C}^\top + \Phi^C(\Delta t_{ij}) \mathbf{R} \Phi^C(\Delta t_{ij})^\top$$

The measurement estimate is thus Gaussian:

$$\hat{\mathbf{z}}_{ij} \sim \mathcal{N}(\mathbf{z}_i^C, \mathbf{V}^C(\Delta t_{ij})),$$

Figure 1 illustrates state propagation and uncertainty in a stable LTI.

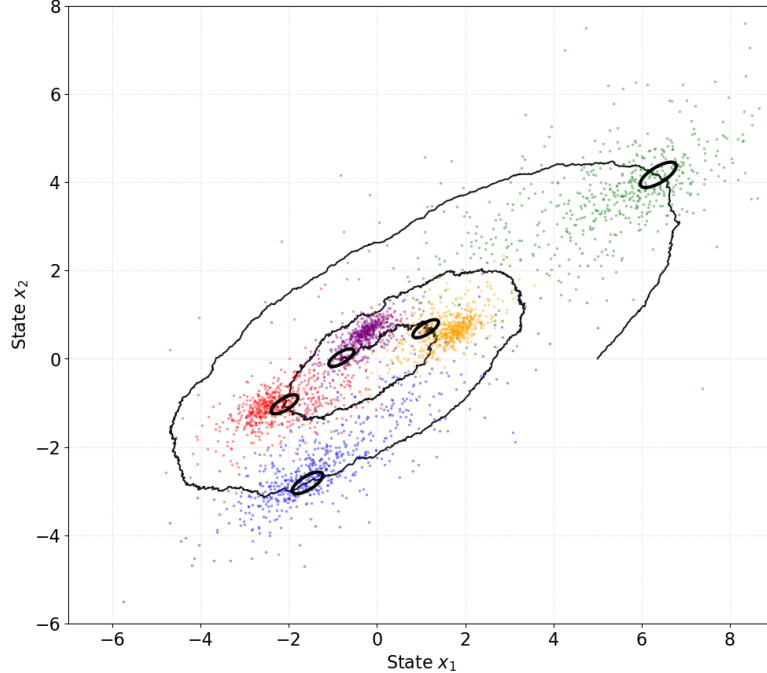


Figure 1. Illustration of uncertainty aggregation in a stable two-dimensional LTI SDE model. The true trajectory is shown in black. For five target points t_i , the plot visualizes the ensemble of estimates $\hat{\mathbf{z}}_{ij}$ mapped through the deterministic transition $e^{\mathbf{A}\Delta t_{ij}}$ from all other noisy measurements ($j \neq i$). The ellipses are centered at the precision-weighted average and scaled by the total posterior covariance $(\sum_j \mathbf{P}_{ij}^C)^{-1}$, representing the estimate's uncertainty. Under stable dynamics, forward propagation (causal) acts as a dissipative filter that attenuates historical noise, while backward propagation (non-causal) amplifies measurement error as the system is integrated against its natural stability.

A.2. Analytical Solution of the Differential Lyapunov Equation (DLE)

For parallel aggregation across all token pairs, we must construct the pairwise propagated precision kernel $\mathbf{P}^C(\Delta t_{ij})$ for all $i, j \in [1, N]$. To obtain an analytically tractable solution, we assume the system matrices are simultaneously diagonalizable by an invertible $\mathbf{S} \in \mathbb{C}^{d \times d}$, where $\mathbf{A} = \mathbf{S}\Lambda\mathbf{S}^{-1}$ and $\mathbf{Q} = \mathbf{S}\Lambda_Q\mathbf{S}^\dagger$. This assumption corresponds to learning dynamics in a basis of decoupled modes.

The forward-propagated state covariance, $\mathbf{V}(\Delta t_{ij})$, is the solution to the DLE (Equation 2):

$$\mathbf{V}(\Delta t_{ij}) = \int_0^{\Delta t_{ij}} e^{\mathbf{A}s} \mathbf{Q} e^{\mathbf{A}^\top s} ds.$$

Transforming to the eigenbasis, the covariance becomes:

$$\mathbf{V}(\Delta t_{ij}) = \mathbf{S}\Lambda\mathbf{V}(\Delta t_{ij})\mathbf{S}^\dagger.$$

where each diagonal entry of $\Lambda_V(\Delta t_{ij})$ satisfies the scalar integral:

$$\lambda_{V,k}(\Delta t_{ij}) = \lambda_{Q,k} \int_0^{\Delta t_{ij}} e^{(\lambda_k + \lambda_k^*)s} ds = \lambda_{Q,k} \int_0^{\Delta t_{ij}} e^{2\operatorname{Re}(\lambda_k)s} ds$$

(where $\Lambda_V = \operatorname{diag}(\lambda_V)$ and $\Lambda_Q = \operatorname{diag}(\lambda_Q)$). Each mode accumulates noise according to its real decay rate $\operatorname{Re}(\lambda_k)$. Modes with weak decay accumulate uncertainty rapidly over time, while strongly damped modes suppress long-range contributions.

Evaluating this integral yields the analytical solution $\varphi(\lambda, \lambda_Q, \Delta t)$ (for the causal case):

$$\Lambda_V(\Delta t_{ij}) = \operatorname{diag}(\varphi(\lambda_k, \lambda_{Q,k}, \Delta t_{ij}))_{k=1}^d,$$

$$\varphi(\lambda, \lambda_Q, \Delta t) = \begin{cases} \lambda_Q \frac{1 - e^{2\operatorname{Re}(\lambda)\Delta t}}{-2\operatorname{Re}(\lambda)}, & \operatorname{Re}(\lambda) \neq 0, \\ \lambda_Q \Delta t, & \operatorname{Re}(\lambda) = 0. \end{cases}$$

A.3. The Measurement Residual and its Covariance

In RFA, the interaction between a query and a key is a statistical comparison between the observer's current state and a past observation propagated through the latent dynamics. We observe a noisy query embedding:

$$\mathbf{z}_i = \mathbf{z}_i^C + \boldsymbol{\varepsilon}_\Gamma, \quad \boldsymbol{\varepsilon}_\Gamma \sim \mathcal{N}(\mathbf{0}, \mathbf{R}_\Gamma),$$

and define the measurement residual:

$$\mathbf{r}_{ij} = \mathbf{z}_i - \Phi^C(\Delta t_{ij})\mathbf{z}_j,$$

which measures disagreement after removing the deterministic evolution predicted by the SDE. Unlike dot-product attention, which compares embeddings in a static feature space, RFA evaluates consistency in the dynamical reference frame of the observer.

Hence, the covariance of the residual consists of two contributions:

$$\mathbf{V}^Z(\Delta t_{ij}) = \underbrace{\mathbf{V}^C(\Delta t_{ij})}_{\text{Propagated (Key) Noise}} + \underbrace{\mathbf{R}_\Gamma}_{\text{Observer (Query) Noise}}.$$

In a global LTI generative model, the same measurement noise would apply to both historical and current observations, i.e. $\mathbf{R} = \mathbf{R}_\Gamma$. Since we instead treat each anchor position as a local estimation problem, we allow the uncertainty of transported observations and the uncertainty of the anchor observation to be modeled separately. The observer noise ensures that precision remains bounded as $\Delta t \rightarrow 0$, reflecting that even perfectly aligned observations are limited by the observer's own uncertainty.

The residual is distributed as:

$$\mathbf{r}_{ij} \sim \mathcal{N}(\mathbf{0}, \mathbf{V}^Z(\Delta t_{ij})).$$

Assuming simultaneous diagonalization of the measurement parameters, $\mathbf{C} = \mathbf{S}\Lambda_C\mathbf{S}^{-1}$, $\mathbf{R} = \mathbf{S}\Lambda_R\mathbf{S}^\dagger$, $\mathbf{R}_\Gamma = \mathbf{S}\Lambda_\Gamma\mathbf{S}^\dagger$, the total covariance decouples in the eigenbasis:

$$\mathbf{V}^Z(\Delta t_{ij}) = \mathbf{S}\Lambda_V^Z(\Delta t_{ij})\mathbf{S}^\dagger.$$

The diagonal matrix $\Lambda_V^Z(\Delta t_{ij})$ is then:

$$\Lambda_V^Z(\Delta t_{ij}) = (\Lambda_C^\dagger \Lambda_C) \Lambda_V(\Delta t_{ij}) + e^{2\operatorname{Re}(\Lambda)\Delta t_{ij}} \Lambda_R + \Lambda_\Gamma$$

This is bounded for all Δt_{ij} in the causal direction if and only if every component of $\operatorname{Re}(\Lambda)$ is negative, i.e., the dynamics are stable.

The required residual precision matrix, $\mathbf{P}^Z(\Delta t_{ij})$, is then obtained by diagonal inversion in the eigenbasis:

$$\mathbf{P}^Z(\Delta t_{ij}) = \mathbf{S}^{-\dagger} \Lambda_P^Z(\Delta t_{ij}) \mathbf{S}^{-1}, \quad \Lambda_P^Z(\Delta t_{ij}) = (\Lambda_V^Z(\Delta t_{ij}))^{-1}.$$

Isotropic Case In particular, consider the isotropic case $\mathbf{A} = -\mu\mathbf{I} + \boldsymbol{\Omega} \in \mathbb{R}^{d \times d}$ where $\mu \in \mathbb{R}^+$ and $\boldsymbol{\Omega} \in \mathbb{R}^{d \times d}$ is diagonalizable over \mathbb{C} , and has strictly imaginary eigenvalues, i.e. $\boldsymbol{\Omega} = \mathbf{S}\boldsymbol{\Lambda}_\Omega\mathbf{S}^{-1}$, where $\mathbf{S} \in \mathbb{C}^{d \times d}$, $\boldsymbol{\Lambda}_\Omega = \text{diag}(\lambda_{\Omega,1}, \dots, \lambda_{\Omega,d})$, with $\lambda_{\Omega,k} \in i\mathbb{R}$. If we also assume that the process and measurement noise are isotropic, $\boldsymbol{\Lambda}_Q = \sigma^2\mathbf{I}$, $\boldsymbol{\Lambda}_R = \eta^2\mathbf{I}$, $\boldsymbol{\Lambda}_\Gamma = \gamma^2\mathbf{I}$, and $\boldsymbol{\Lambda}_C = \lambda_C\mathbf{I}$. Then:

$$\boldsymbol{\Lambda}_V^Z(\Delta t_{ij}) = \sigma_V^2(\Delta t_{ij})\mathbf{I}, \quad \sigma_V^2(\Delta t_{ij}) := |\lambda_C|^2 \sigma^2 \frac{1 - e^{-2\mu\Delta t_{ij}}}{2\mu} + e^{-2\mu\Delta t_{ij}}\eta^2 + \gamma^2$$

Collecting terms, we can express the kernel in the form:

$$\sigma_V^2(\tau) = \alpha e^{-2\mu\tau} + \beta,$$

where:

$$\alpha = \eta^2 - \tilde{\sigma}^2, \quad \beta = \gamma^2 + \tilde{\sigma}^2, \quad \tilde{\sigma}^2 := |\lambda_C|^2 \frac{\sigma^2}{2\mu}$$

As $\tau \rightarrow \infty$, the variance saturates at the total uncertainty floor β . The sign of α dictates the qualitative evolution of the observer's uncertainty:

- **Integrative (Denoising) Regime ($\alpha > 0$)**: Occurs when the initial measurement noise is high $\eta^2 > \tilde{\sigma}^2$. The variance decays from its initial peak toward the equilibrium floor β , representing a system that “settles” into a more reliable latent state as transient measurement noise is filtered out by the stable dynamics.
- **Diffusive (Forgetting) Regime ($\alpha < 0$)**: Occurs when steady-state process uncertainty exceeds the measurement noise variance: $\tilde{\sigma}^2 > \eta^2$. As the temporal lag τ increases, the variance grows toward the steady-state floor β , representing the “blurring” of historical information.

In the integrative regime, zero process noise is statistically equivalent to larger measurement noise, since both produce the same steady-state uncertainty, so the noise decomposition becomes non-identifiable. The utility of modeling process noise is that it allows a model to learn to represent the diffusive regime.

The Mahalanobis Distance To evaluate residuals under this conditional model, we use the Mahalanobis distance d_{ij}^2 , which normalizes the error by the total propagated covariance \mathbf{V}_{ij}^Z :

$$d_{ij}^2 := \mathbf{r}_{ij}^\top \mathbf{P}_{ij}^Z \mathbf{r}_{ij}.$$

This measures the size of the residual relative to the uncertainty predicted by the SDE prior. Large values indicate that the propagated observation is statistically inconsistent with the anchor state, given the uncertainty accumulated over Δt_{ij} .

A.4. Local Conditional Estimation Under Observable Residual Noise

Under the linear SDE prior, the exact likelihood of the full measurement sequence induces dense temporal correlations, requiring sequential inference (e.g., Kalman filtering). To obtain a parallel estimator, we approximate the likelihood by treating transported observations as conditionally independent given the latent anchor state \mathbf{z}_i^C :

$$p(\{\hat{\mathbf{z}}_{ij}\}_{j \leq i}, \mathbf{z}_i | \mathbf{z}_i^C) \approx p(\mathbf{z}_i | \mathbf{z}_i^C) \prod_{j \leq i} p(\hat{\mathbf{z}}_{ij} | \mathbf{z}_i^C),$$

which ignores cross-covariances induced by shared process noise.

Rather than explicitly estimating the latent anchor state \mathbf{z}_i^C , we instead evaluate the marginal likelihood of the observable residuals $\mathbf{r}_{ij} = \mathbf{z}_i - \hat{\mathbf{z}}_{ij}$. Since \mathbf{z}_i and $\hat{\mathbf{z}}_{ij}$ are, by assumption, independent noisy observations of the same latent state, the residual is distributed as:

$$\mathbf{r}_{ij} \sim \mathcal{N}\left(\mathbf{0}, \mathbf{V}_{ij}^C + \mathbf{R}_\Gamma\right), \quad \mathbf{P}_{ij}^Z = \left(\mathbf{V}_{ij}^C + \mathbf{R}_\Gamma\right)^{-1},$$

where \mathbf{P}_{ij}^Z denotes the precision of the observable residual.

We then seek an estimate \bar{z}_i that minimizes the sum of squared Mahalanobis distances:

$$\bar{z}_i = \arg \min_{\mathbf{z}_i} \sum_{j \leq i} (\mathbf{z}_i - \hat{\mathbf{z}}_{ij})^\top \mathbf{P}_{ij}^Z (\mathbf{z}_i - \hat{\mathbf{z}}_{ij}),$$

Setting the gradient to zero yields the precision-weighted batch estimator:

$$\bar{z}_i = \left(\sum_{j \leq i} \mathbf{P}_{ij}^Z \right)^{-1} \sum_{j \leq i} \mathbf{P}_{ij}^Z \hat{\mathbf{z}}_{ij}.$$

This reduction enables parallel $\mathcal{O}(N^2)$ aggregation.

Remark on Approximation Validity. The conditional independence approximation is supported by the SDE dynamics in two complementary limits, defined by the ratio of steady-state process uncertainty to measurement noise, $\mathcal{R} := \tilde{\sigma}^2/\eta^2$.

Integrative Limit ($\mathcal{R} \ll 1$). Strong dissipation and low process noise suppress cross-temporal correlations.

Diffusive Limit ($\mathcal{R} \gg 1$). Although temporal correlations increase, the marginal precisions \mathbf{P}_{ij}^Z decay rapidly with temporal lag as uncertainty accumulates. This induces an implicit self-regularization: distant tokens—those for which independence is least accurate—receive negligible weight under the SDE prior.

A.5. Robust State Estimation

The estimator in Section A.4 weights each transported observation according to its predicted uncertainty under the SDE prior. This accounts for temporal reliability, but the weights are independent of the observed residuals. We therefore introduce data-dependent reweighting based on statistical consistency with the anchor state.

To incorporate this effect, we reweight the SDE-derived precision by a scalar function of the Mahalanobis distance:

$$\tilde{\mathbf{P}}_{ij} = w(d_{ij}^2) \mathbf{P}_{ij}^Z, \quad d_{ij}^2 = \mathbf{r}_{ij}^\top \mathbf{P}_{ij}^Z \mathbf{r}_{ij}.$$

This preserves the analytically derived temporal kernel while introducing data-dependent reweighting based on statistical consistency with the predicted state.

Since the squared Mahalanobis distance d_{ij}^2 depends on the unknown anchor estimate, the resulting weights w_{ij} are implicitly functions of \bar{z}_i . The corresponding update therefore defines a fixed-point equation that can be interpreted as one step of an iteratively reweighted least-squares (IRLS) procedure (see Appendix C.3).

Given a current estimate (or proxy) of the anchor state \mathbf{z}_i , the reweighted update takes the form:

$$\bar{z}_i = \left(\sum_{j \leq i} w_{ij} \mathbf{P}_{ij}^Z \right)^{-1} \sum_{j \leq i} w_{ij} \mathbf{P}_{ij}^Z \hat{\mathbf{z}}_{ij}, \quad w_{ij} = w(d_{ij}^2).$$

In practice, RFA applies this reweighted aggregation once per layer, yielding an efficient approximation to robust state estimation while preserving full parallelism.

A.5.1. ROBUST INFLUENCE FUNCTIONS FOR PRECISION REWEIGHTING

The choice of $w(\cdot)$ determines how strongly inconsistent observations are down-weighted and thus defines the estimator's robustness profile.

A natural baseline is an exponential influence function,

$$w_{ij} \propto \exp\left(-\frac{d_{ij}^2}{\nu}\right),$$

which recovers the functional form of Softmax attention with temperature ν . However, exponential decay assigns negligible weight to moderately inconsistent observations, yielding brittle, winner-take-all behavior under low signal-to-noise.

To obtain heavier tails, we adopt a power-law family of influence functions,

$$w_{ij} \propto \left(1 + \frac{d_{ij}^2}{\nu}\right)^{-\kappa},$$

where $\kappa > 0$ controls the rate at which inconsistent observations are suppressed. This form mitigates the influence of outliers, which also helps reduce the overconfidence induced by the conditional independence approximation.

A.6. Parallel Aggregation via Diagonalization

To obtain a scalable implementation, we transform the robust precision-weighted estimator to the eigenbasis in which the propagated precision is diagonal. We define the state and propagated measurements in this basis as:

$$\mathbf{z}_{s,i} := \mathbf{S}^{-1} \mathbf{z}_i, \quad \hat{\mathbf{z}}_{s,ij} := e^{\Lambda \Delta t_{ij}} \mathbf{z}_{s,j}.$$

Using the simultaneous diagonalization $\mathbf{P}_{ij}^Z = \mathbf{S}^{-\dagger} \Lambda_{\mathbf{P}}^Z(\Delta t_{ij}) \mathbf{S}^{-1}$, the Mahalanobis distance decomposes into independent scalar components:

$$d_{ij}^2 = (\mathbf{z}_{s,i} - \hat{\mathbf{z}}_{s,ij})^\dagger \Lambda_{\mathbf{P},ij}^Z (\mathbf{z}_{s,i} - \hat{\mathbf{z}}_{s,ij}) = \sum_{k=1}^d \lambda_{\mathbf{P},k}^Z(\Delta t_{ij}) |z_{s,i,k} - \hat{z}_{s,ij,k}|^2.$$

This allows the robust weights $w_{ij} = w(d_{ij}^2)$ to be computed efficiently for all token pairs.

Applying the robust reweighted estimator in this basis yields:

$$\bar{\mathbf{z}}_{s,i} = \left(\sum_{j \leq i} w_{ij} \Lambda_{\mathbf{P},ij}^Z \right)^{-1} \sum_{j \leq i} w_{ij} \Lambda_{\mathbf{P},ij}^Z \hat{\mathbf{z}}_{s,ij}.$$

Since all matrices are diagonal, both the sum and inverse are element-wise operations.

Writing $\boldsymbol{\lambda}_{\mathbf{P},ij}^Z := \text{diag}(\Lambda_{\mathbf{P},ij}^Z)$, we define the unnormalized attention weights as:

$$\tilde{\mathcal{A}}_{ij} := w_{ij} \boldsymbol{\lambda}_{\mathbf{P},ij}^Z,$$

and the normalized weights as:

$$\mathcal{A}_{ij} = \tilde{\mathcal{A}}_{ij} \oslash \left(\sum_{j' \leq i} \tilde{\mathcal{A}}_{ij'} \right),$$

where \oslash denotes element-wise division. The aggregation then takes the familiar attention form:

$$\bar{\mathbf{z}}_{s,i} = \sum_{j \leq i} \mathcal{A}_{ij} \odot \hat{\mathbf{z}}_{s,ij}.$$

Finally, the output in the original coordinate system is recovered by $\bar{\mathbf{z}}_i = \mathbf{S} \bar{\mathbf{z}}_{s,i}$. All operations are $\mathcal{O}(d)$ per token pair, yielding an overall complexity of $\mathcal{O}(N^2 d)$ with no matrix inversions.

Equivalently, this normalization can be written in Softmax form by defining dimension-wise attention logits. For Gaussian reweighting $w_{ij} \propto \exp(-d_{ij}^2/\nu)$, the logit becomes:

$$\ell_{ij,k} := \log \lambda_{\mathbf{P},k}^Z(\Delta t_{ij}) - \frac{1}{\nu} \lambda_{\mathbf{P},k}^Z(\Delta t_{ij}) |r_{s,ij,k}|^2,$$

yielding:

$$\mathcal{A}_{ij,k} = \frac{\exp(\ell_{ij,k})}{\sum_{j' \leq i} \exp(\ell_{ij',k})}.$$

For the power law influence function $w_{ij} \propto (1 + d_{ij}^2/\nu)^{-\kappa}$, the corresponding logit becomes:

$$\ell_{ij,k} := \log \lambda_{\mathbf{P},k}^Z(\Delta t_{ij}) - \kappa \log \left(1 + \frac{1}{\nu} \lambda_{\mathbf{P},k}^Z(\Delta t_{ij}) |r_{s,ij,k}|^2 \right),$$

This defines a Softmax-style aggregation over heavy-tailed consistency scores, yielding robust attention under model mismatch and non-Gaussian noise.

In the isotropic case where $\lambda_{\mathbf{P},k}^Z(\Delta t_{ij}) = \lambda_{\mathbf{P},ij}^Z$ is a shared scalar across dimensions, both kernels reduce to scalar logits:

$$\ell_{ij} = \log(\lambda_{\mathbf{P},ij}^Z) - \frac{1}{\nu} \lambda_{\mathbf{P},ij}^Z \|r_{ij}\|^2 \quad (\text{Gaussian}),$$

which is a Softmax normalization over scalar similarity scores.

A.6.1. LIKELIHOOD-CALIBRATED ATTENTION IN THE ISOTROPIC CASE

Under an isotropic covariance constraint:

$$\mathbf{V}_{ij}^Z = \sigma_V^2(\Delta t_{ij}) \mathbf{I}_d,$$

where $\sigma_V^2(\Delta t_{ij}) \in \mathbb{R}^+$, the robust precision-reweighted attention score may be written as:

$$\log \tilde{w}_{ij} = -\log(\sigma_V^2(\Delta t_{ij})) - \kappa \log\left(1 + \frac{1}{\nu} d_{ij}^2\right),$$

where $d_{ij}^2 = \|\mathbf{r}_{ij}\|^2 / \sigma_V^2(\Delta t_{ij})$ is the isotropic Mahalanobis distance.

Choosing $\kappa = \frac{\nu+d}{d}$ makes this expression proportional (up to additive constants) to the dimension-normalized negative log-likelihood of an isotropic multivariate Student's t distribution:

$$\mathcal{L}_{ij} = -\log(\sigma_V^2(\Delta t_{ij})) + \frac{\nu+d}{d} \log\left(1 + \frac{1}{\nu} d_{ij}^2\right).$$

Thus, in the isotropic case, robust precision-weighted filtering with power-law influence and exponent $\kappa = (\nu + d)/d$ is equivalent (up to constants) to using dimension-normalized Student- t log-likelihoods as attention logits.

The dimension normalization is critical for stability: in high-dimensional spaces, squared Mahalanobis distances concentrate, causing unnormalized likelihoods to produce overly sharp, near-deterministic weights. Normalizing by dimension preserves sensitivity to relative consistency rather than absolute norm.

In the limit $d \rightarrow \infty$, the exponent satisfies $\kappa \rightarrow 1$, and the influence function reduces to the standard rational form of an M-estimator:

$$w_{ij} \propto (1 + d_{ij}^2 / \nu)^{-1}.$$

B. Robust Filter Attention Mechanism

B.1. Anisotropic Tensor RFA (Naive Implementation)

We first present an Anisotropic Tensor formulation of RFA, representing the most general form implied by our derivation under diagonalizable dynamics. Although it is not scalable due to its $\mathcal{O}(N^2d)$ memory cost, it provides the reference estimator from which an efficient variant is derived.

B.1.1. LEARNED CHANGE-OF-BASIS PROJECTIONS

The transformation to the decoupled eigenbasis is learned directly through complex-valued projections. We define:

$$\mathbf{W}_Q, \mathbf{W}_K, \mathbf{W}_V, \mathbf{W}_O \in \mathbb{C}^{d \times d},$$

where d is the embedding dimension. The input projections $\{\mathbf{W}_Q, \mathbf{W}_K, \mathbf{W}_V\}$ parameterize the learned diagonalizing basis \mathbf{S}^{-1} , mapping the real-world input into the complex latent frame where the DLE is analytically solvable. Conversely, the output projection \mathbf{W}_O parameterizes the reconstruction basis \mathbf{S} , mapping the filtered state estimate back into the original embedding space.

Given input sequence $\mathbf{Z} \in \mathbb{R}^{d \times N}$, we obtain the latent representations:

$$\mathbf{Q} = \mathbf{W}_Q \mathbf{Z}, \quad \mathbf{K} = \mathbf{W}_K \mathbf{Z}, \quad \mathbf{V} = \mathbf{W}_V \mathbf{Z}.$$

B.1.2. LATENT PROPAGATION VIA LINEAR DYNAMICS

The SDE framework allows for separate dynamics and noise parameters $\{\boldsymbol{\lambda}, \boldsymbol{\lambda}_Q, \boldsymbol{\lambda}_R, \boldsymbol{\lambda}_\Gamma, \boldsymbol{\lambda}_C\}$ for the query/key and value latent spaces, allowing independent modeling of the precision prior and the precision used in the Mahalanobis distance. For simplicity and parameter efficiency, we instead use a shared embedding dimension d and a unified set of parameters.

In this reference model, every feature k possesses its own complex eigenvalue λ_k , allowing the model to learn a bank of filters with diverse damping rates and resonant frequencies. We define the propagation tensors \mathcal{E} and the resulting conditional means $\hat{\mathcal{V}}$:

$$\mathcal{E}[k, i, j] = e^{\boldsymbol{\lambda}_k(t_i - t_j)}, \quad \hat{\mathcal{V}}[k, i, j] = \mathcal{E}[k, i, j] \cdot \mathbf{V}[k, j].$$

B.1.3. MEASUREMENT RESIDUALS & PRECISION

We compute the measurement residual tensor \mathcal{R}_{qk} :

$$\mathcal{R}_{qk}[k, i, j] = \mathbf{Q}[k, i] - \mathcal{E}[k, i, j] \cdot \mathbf{K}[k, j],$$

This is weighted by the analytic precision tensor \mathcal{P}^Z , which is defined element-wise for each channel k using the DLE solution:

$$\mathcal{P}^Z[k, i, j] = \left(\tilde{\sigma}_k^2 (1 - e^{-2\mu_k \Delta t_{ij}}) + \eta_k^2 e^{-2\mu_k \Delta t_{ij}} + \gamma_k^2 \right)^{-1},$$

where $\mu_k = -\text{Re}(\lambda_k)$.

B.1.4. AGGREGATION

Unlike standard attention, which applies a single scalar score per head, tensor RFA computes an attention tensor $\mathcal{A} \in \mathbb{R}^{d \times N \times N}$. This enables independent, precision-weighted routing for every individual feature dimension. The score tensor combines a dimension-specific precision prior with a shared robust residual penalty:

$$\mathcal{L}[k, i, j] = \log(\mathcal{P}^Z[k, i, j]) - \kappa \log \left(1 + \frac{1}{\nu} \sum_{k'} \mathcal{P}^Z[k', i, j] \cdot |\mathcal{R}_{qk}[k', i, j]|^2 \right).$$

The final estimate is computed via a row-wise Softmax over the logits, followed by a precision-weighted aggregation:

$$\mathcal{A}[k, i, j] = \text{Softmax}_j(\mathcal{L}[k, i, j]), \quad \bar{\mathbf{V}}[k, i] = \sum_{j \leq i} \mathcal{A}[k, i, j] \cdot \hat{\mathcal{V}}[k, i, j].$$

The final estimate is then projected back to the real-valued embedding space:

$$\bar{\mathbf{Z}} = \text{Re}(\mathbf{W}_O \bar{\mathbf{V}}).$$

The time complexity remains $\mathcal{O}(N^2d)$, but storing the conditional means, residuals, and attention tensors requires $\mathcal{O}(N^2d)$ memory, limiting scalability. We therefore derive a memory-efficient implementation that avoids explicit tensor storage.

B.2. Complexity Reduction via Factorization

We introduce the following factorizations to simplify the computation:

B.2.1. TOEPLITZ KERNEL FOR PRECISION

If the measurements occur at equal time intervals δt , the analytic precision kernel $\mathcal{P}^Z[k, i, j]$ depends only on the channel k and the time lag $\tau = |i - j|$. This induces a Toeplitz structure along the temporal dimensions for each channel.

Letting $\Delta t_{ij} = \tau \delta t$, we can thus pre-compute 1D covariance and precision kernels: $\mathcal{K}^V \in \mathbb{R}^{d \times N}$:

$$\mathcal{K}^V[k, \tau] = \tilde{\sigma}_k^2 (1 - e^{-2\mu_k \delta t \tau}) + \eta_k^2 e^{-2\mu_k \delta t \tau} + \gamma_k^2,$$

The full precision tensor is then simply the element-wise inverse of this kernel:

$$\mathcal{P}^Z[k, i, j] = \mathcal{K}^P[k, |i - j|] := 1/\mathcal{K}^V[k, |i - j|].$$

B.2.2. FACTORIZING THE CONDITIONAL MEANS

Because the dynamics are LTI, we can avoid explicitly constructing $\mathcal{O}(N^2d)$ estimates by decomposing the transition factor \mathcal{E} into separate forward and backward transition factors for each dimension k :

$$\mathcal{E}[k, i, j] = \Phi^+[k, i] \cdot \Phi^-[k, j], \quad \text{where:} \quad \Phi^+[k, i] := e^{\lambda_k t_i}, \quad \Phi^-[k, i] := e^{-\lambda_k t_i}.$$

We can then define stationary representations:

$$\hat{\mathbf{Q}}[k, j] := \Phi^-[k, j] \cdot \mathbf{Q}[k, j], \quad \hat{\mathbf{K}}[k, j] := \Phi^-[k, j] \cdot \mathbf{K}[k, j], \quad \hat{\mathbf{V}}[k, j] := \Phi^-[k, j] \cdot \mathbf{V}[k, j].$$

The conditional means are then refactored as products:

$$\hat{\mathcal{K}}[k, i, j] = \Phi^+[k, i] \cdot \hat{\mathbf{K}}[k, j], \quad \hat{\mathcal{V}}[k, i, j] = \Phi^+[k, i] \cdot \hat{\mathbf{V}}[k, j]$$

This reduces the memory requirement from $\mathcal{O}(N^2d)$ to $\mathcal{O}(Nd)$.

Since $\Phi^+[k, i]$ does not depend on j , we can pull it outside the sum:

$$\bar{\mathbf{V}}[k, i] := \sum_{j \leq i} \mathcal{A}[k, i, j] \cdot \hat{\mathcal{V}}[k, i, j] = \Phi^+[k, i] \cdot \sum_{j \leq i} \mathcal{A}[k, i, j] \cdot \hat{\mathbf{V}}[k, j]$$

B.2.3. MEMORY AND STABILITY CONSTRAINTS

Recall that:

$$\mathcal{R}_{qk}[k, i, j] = \mathbf{Q}[k, i] - \hat{\mathcal{K}}[k, i, j]$$

Plugging in the factorizations for $\hat{\mathbf{Q}}[k, j]$ and $\hat{\mathcal{K}}[k, i, j]$, the residual becomes:

$$\mathcal{R}_{qk}[k, i, j] = \mathbf{Q}[k, i] - \Phi^+[k, i] \cdot \hat{\mathbf{K}}[k, j] = \Phi^+[k, i] \cdot (\hat{\mathbf{Q}}[k, i] - \hat{\mathbf{K}}[k, j]).$$

The Mahalanobis distance now becomes:

$$\mathbf{D}^2[i, j] = \sum_k \underbrace{\mathcal{K}^P[k, |i - j|]}_{\text{Precision kernel}} \cdot \underbrace{|\Phi^+[k, i]|^2}_{\text{Forward decay}} \cdot \left[\underbrace{|\hat{\mathbf{Q}}[k, i]|^2}_{\text{Stationary Query}} + \underbrace{|\hat{\mathbf{K}}[k, j]|^2}_{\text{Stationary Key}} - \underbrace{2 \text{Re}(\hat{\mathbf{Q}}^*[k, i] \hat{\mathbf{K}}[k, j])}_{\text{Stationary Cross-term}} \right].$$

The remaining bottleneck is the k -dependence of the precision kernel \mathcal{K}^P in the evaluation of the cross-term:

$$\sum_k \mathcal{K}^P[k, |i - j|] \cdot 2 \operatorname{Re}(\hat{\mathbf{Q}}^*[k, i] \hat{\mathbf{K}}[k, j]).$$

In standard attention, scores are computed with a single matrix multiplication $(\mathbf{Q}\mathbf{K}^\top)$. Here, however, the precision kernel $\mathcal{K}^P[k, |i - j|]$ weights each feature differently as a function of time lag, so the summation over k cannot be expressed as a single matmul. Consequently, computing this term for all (i, j) pairs does not admit a reduction in memory or bandwidth without additional structure. Achieving $\mathcal{O}(N^2 + Nd)$ memory therefore requires the precision kernel to be independent of the feature index k , allowing it to factor outside the summation.

A degenerate case occurs in the zero-noise limit, where uncertainty no longer accumulates with temporal separation and the precision kernel becomes independent of $|i - j|$. This recovers a memory-efficient formulation with anisotropic (feature-wise) decay, similar to `xPos`.

However, for stable dynamics with $\mu_k > 0$, the backward transition factor $\Phi^-[k, j] = e^{(\mu_k - i\omega_k)t_j}$ grows exponentially with sequence length. When decay rates vary across features, the stationary representations $\hat{\mathbf{Q}}, \hat{\mathbf{K}}, \hat{\mathbf{V}}$ grow exponentially with sequence length, making fully parallel computation numerically unstable because forward and backward factors cancel only after multiplication, allowing intermediate values to overflow.

Therefore, retaining a non-constant precision kernel while ensuring numerical stability under extrapolation requires restricting decay to be isotropic within each head. This allows decay to be factored at the head level rather than per feature, enabling stable, fully parallel attention with $\mathcal{O}(N^2 + Nd)$ memory. This motivates the Isotropic RFA variant introduced next.

B.3. The Scalable Isotropic RFA Mechanism

B.3.1. ISOTROPIC DECAY AND NOISE ASSUMPTIONS

All assumptions in this section are applied *per attention head*. In particular, the real part of the eigenvalues within a head is taken to be a shared scalar $-\mu$:

$$\lambda_k = -\mu + i\omega_k, \quad \mu \in \mathbb{R}^+, \omega_k \in \mathbb{R}$$

This corresponds to a system with an isotropic plus skew-symmetric state matrix ($\Omega = -\Omega^\top \in \mathbb{R}^{d \times d}$),

$$\mathbf{A} = -\mu \mathbf{I} + \Omega,$$

We also assume that the noise is isotropic, i.e. that the noise covariances are scalar multiples of identity:

$$\mathbf{\Lambda}_Q = \sigma^2 \mathbf{I}, \quad \mathbf{\Lambda}_R = \eta^2 \mathbf{I}, \quad \mathbf{\Lambda}_\Gamma = \gamma^2 \mathbf{I}$$

Under this constraint, the covariance kernels simplify to scalar functions:

$$\sigma_{\mathbf{V}}^2(|i - j|) = \tilde{\sigma}^2 (1 - e^{-2\mu\delta t|i - j|}) + \eta^2 e^{-2\mu\delta t|i - j|} + \gamma^2$$

Hence, the precision kernel becomes a scalar function of the time lag $\tau = |i - j|$, allowing it to be pulled outside the feature summation. Defining $\mathbf{V}_{\Delta t}[i, j] := \sigma_{\mathbf{V}}^2(|i - j|)$ and $\mathbf{P}_{\Delta t}[i, j] := 1/\mathbf{V}_{\Delta t}[i, j]$, the matrix of Mahalanobis distances become:

$$\mathbf{D}^2[i, j] = \mathbf{P}_{\Delta t}[i, j] \cdot \left(\sum_k |\mathcal{R}_{\mathbf{qk}}[k, i, j]|^2 \right) =: \mathbf{P}_{\Delta t}[i, j] \cdot \|\mathbf{R}_{\mathbf{qk}}[i, j]\|^2,$$

(Note that $\|\mathbf{R}_{\mathbf{qk}}\|$ denotes a matrix of vector norms, not a matrix norm.)

B.3.2. SIMPLIFYING THE SQUARED RESIDUAL NORM

The isotropic constraint allows the dynamics to be factored into a stable decay term and complex forward/backward rotations:

$$\mathbf{E}[i, j] = e^{-\mu|t_i - t_j|}, \quad \tilde{\Phi}^+[k, i] := e^{i\omega_k t_i}, \quad \tilde{\Phi}^-[k, i] := e^{-i\omega_k t_i},$$

We can then define backward-rotated queries, keys, and values:

$$\tilde{\mathbf{Q}} := \tilde{\Phi}^- \odot \mathbf{Q}, \quad \tilde{\mathbf{K}} := \tilde{\Phi}^- \odot \mathbf{K}, \quad \tilde{\mathbf{V}} := \tilde{\Phi}^- \odot \mathbf{V},$$

Note that:

$$\Phi^+[k, i] = e^{-\mu t_i} \tilde{\Phi}^+[k, i], \quad \hat{Q}[k, i] = e^{\mu t_i} \tilde{Q}[k, i], \quad \hat{K}[k, j] = e^{\mu t_j} \tilde{K}[k, j].$$

Plugging this into the expression for the Mahalanobis distance, and using the fact that complex rotation preserves magnitude:

$$\begin{aligned} \|\mathbf{R}_{qk}[i, j]\|^2 &= \sum_k e^{-2\mu t_i} |\tilde{\Phi}^+[k, i]|^2 \cdot \left[e^{2\mu t_i} |\tilde{Q}[k, i]|^2 + e^{2\mu t_j} |\tilde{K}[k, j]|^2 - 2e^{\mu t_i} e^{\mu t_j} \operatorname{Re}(\tilde{Q}^*[k, i] \tilde{K}[k, j]) \right]. \\ &= \sum_k \left[|\tilde{Q}[k, i]|^2 + e^{-2\mu(t_i - t_j)} |\tilde{K}[k, j]|^2 - 2e^{-\mu(t_i - t_j)} \operatorname{Re}(\tilde{Q}[k, i]^* \tilde{K}[k, j]) \right]. \end{aligned}$$

Or, in vectorized form:

$$\|\mathbf{R}_{qk}[i, j]\|^2 = \underbrace{\|\mathbf{Q}_i\|^2}_{\text{Query Energy}} + \underbrace{\mathbf{E}[i, j]^2 \|\mathbf{K}_j\|^2}_{\text{Decayed Key Energy}} - \underbrace{2 \mathbf{E}[i, j] \operatorname{Re}(\tilde{Q}_i^\dagger \tilde{K}_j)}_{\text{Propagated Cross-term}}$$

(since $\|\mathbf{Q}_i\|^2 = \|\tilde{Q}_i\|^2$ and $\|\mathbf{K}_i\|^2 = \|\tilde{K}_i\|^2$).

The cross-term $\operatorname{Re}(\tilde{Q}^\dagger \tilde{K})$ is computed using one $\mathcal{O}(N^2 d)$ matrix multiplication, achieving the required memory efficiency.

B.3.3. THE ATTENTION MATRIX AND ESTIMATE

The score matrix \mathbf{L} is defined using the negative log-likelihood of the robust M-estimator, which combines the uncertainty prior $\mathbf{V}_{\Delta t}$ and the squared Mahalanobis distance $\mathbf{P}_{\Delta t} \odot \|\mathbf{R}_{qk}\|^2$. Letting $\kappa = \frac{\nu+d}{d}$, this is:

$$\mathbf{L} = \log(\mathbf{P}_{\Delta t}) - \frac{\nu+d}{d} \log \left(1 + \frac{1}{\nu} \mathbf{P}_{\Delta t} \odot \|\mathbf{R}_{qk}\|^2 \right).$$

Defining a causal mask $\mathbf{M}_{\text{causal}}$, we can then express the row-normalization using row-wise Softmax:

$$\hat{\mathbf{A}}[i, j] = \operatorname{Softmax}_j(\mathbf{L}[i, j] + \mathbf{M}_{\text{causal}})$$

The value aggregation is refactored for stability:

$$\begin{aligned} \bar{\mathbf{V}}[k, i] &= \left(e^{-\mu t_i} \tilde{\Phi}^+[k, i] \right) \cdot \sum_{j \leq i} \hat{\mathbf{A}}[i, j] \cdot \left(e^{\mu t_j} \tilde{\mathbf{V}}[k, j] \right) \\ &= \tilde{\Phi}^+[k, i] \cdot \sum_{j \leq i} (\hat{\mathbf{A}}[i, j] \cdot \mathbf{E}[i, j]) \cdot \tilde{\mathbf{V}}[k, j] \end{aligned}$$

Hence, defining a decayed attention matrix $\mathbf{A} := \hat{\mathbf{A}} \odot \mathbf{E}$, the filtered estimate $\bar{\mathbf{V}}$ is computed by transforming the aggregation back into the forward-rotated frame:

$$\bar{\mathbf{V}} = \tilde{\Phi}^+ \odot (\tilde{\mathbf{V}} \mathbf{A}^\top).$$

Or, in a form more typical for attention:

$$\bar{\mathbf{V}}^\top = (\tilde{\Phi}^+)^{\top} \odot (\mathbf{A} \tilde{\mathbf{V}}^\top)$$

This rotate-aggregate-rotate-back structure ensures that the value aggregation is equivariant to temporal shifts, allowing the model to preserve the dynamical phase relationships of the SDE regardless of the absolute position in the sequence (Fig. 2).

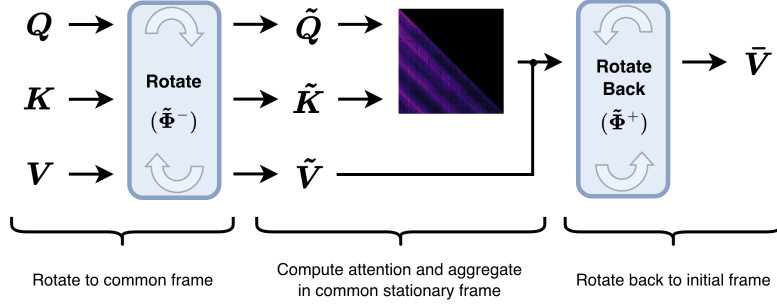


Figure 2. Rotate, aggregate, rotate-back structure of Isotropic RFA. Queries, keys, and values are rotated into a common frame to compute attention and aggregate values. The resulting estimate is then rotated back to the initial frame, yielding a state that preserves relative phase while remaining equivariant to absolute position.

B.4. A Physical Interpretation of Positional Embeddings

B.4.1. LEARNABLE GATES AND PHYSICAL PHASE TRANSITIONS

RFA's behavior is fundamentally determined by the balance between initial measurement uncertainty (η^2) and the steady-state process uncertainty accumulated through stochastic drift. We characterize this balance through the combined noise coefficients:

$$\alpha = \eta^2 - \tilde{\sigma}^2, \quad \beta = \gamma^2 + \tilde{\sigma}^2, \quad \tilde{\sigma}^2 := |\lambda_C|^2 \frac{\sigma^2}{2\mu}$$

In particular, the sign of α defines a phase transition between a *Diffusive* and an *Integrative* regime. Note that the model is constrained by the physical reality that the total steady-state uncertainty β must always bound the transient components ($|\alpha| \leq \beta$), ensuring strictly positive variances.

Here, we examine the behavior of the additive bias $B_{\Delta t} := \log(P_{\Delta t})$ and the multiplicative gating term $P_{\Delta t}$. The behavior of each regime is illustrated in Fig 3, and the effect of the decay is shown in Fig 4.

I. The Diffusive (Forgetting) Regime ($\alpha < 0$) In this regime, stochastic drift accumulates faster than the initial signal settles, representing a system where process uncertainty grows over time. Memory is aggressively eroded by stochastic drift as the temporal lag Δt increases.

Additive Bias ($B_{\Delta t}$): Acts as a Forgetting Prior. Letting $\alpha' = -\alpha > 0$, the bias follows a logarithmic decay:

$$B_{\Delta t} = -\log(\beta) - \log\left(1 - \frac{\alpha'}{\beta} e^{-2\mu\Delta t}\right).$$

The bias starts at its maximum value at $\Delta t = 0$ and decays toward a floor of $-\log(\beta)$ as $\Delta t \rightarrow \infty$.

Multiplicative Gate ($P_{\Delta t}$): Functions as a Closing Gate. The precision decays as:

$$P_{\Delta t} = (\beta - \alpha' e^{-2\mu\Delta t})^{-1}$$

Selectivity is maximal at $\Delta t \approx 0$ and rapidly blurs out as the lag between tokens increases.

II. The Integrative (Denoising) Regime ($\alpha > 0$) Here, initial measurement noise (η^2) is the primary error source. The SDE dynamics settle faster than drift accumulates, allowing the model to denoise the signal.

Additive Bias ($B_{\Delta t}$): Acts as a Settling Prior. The bias follows a mirrored Softplus:

$$B_{\Delta t} = -\log(\beta) - \text{softplus}(\ln(\alpha/\beta) - 2\mu\Delta t).$$

The budget for the token starts low and curves up toward its maximum as key-side measurement noise η^2 dissipates.

Multiplicative Gate ($P_{\Delta t}$): Functions as an Opening Gate. The precision follows a sigmoid:

$$P_{\Delta t} = \frac{1}{\beta} \cdot \text{sigmoid}(2\mu\Delta t - \ln(\alpha/\beta)).$$

Selectivity is low initially to avoid over-committing to a noisy initial observation, with the gate waiting until the signal settles into a reliable latent position to open.

RFA parameterizes both regimes through the same learned noise variances $(\tilde{\sigma}^2, \eta^2, \gamma^2)$, allowing attention heads to move smoothly between diffusive and integrative behavior during training.

B.4.2. THE ZERO-DECAY LIMIT

If the queries and keys are normalized, the matrix of squared residual norms becomes:

$$\|\mathbf{R}_{qk}\|^2 = \mathbf{1} + \mathbf{E}^2 - 2\mathbf{E} \odot \text{Re}(\tilde{\mathbf{Q}}^\dagger \tilde{\mathbf{K}}).$$

In the zero-decay limit ($\mu \rightarrow 0$), the relative decay vanishes ($\mathbf{E} = \mathbf{1}$), and the residual simplifies to the chordal distance on the unit-norm hypersphere:

$$\|\mathbf{R}_{qk}\|^2 = 2(1 - \text{Re}(\tilde{\mathbf{Q}}^\dagger \tilde{\mathbf{K}})).$$

Substituting this into the NLL,

$$\mathbf{L} = \log(\mathbf{P}_{\Delta t}) - \kappa \log \left(1 + \frac{2}{\nu} \mathbf{P}_{\Delta t} - \frac{2}{\nu} \mathbf{P}_{\Delta t} \odot \text{Re}(\tilde{\mathbf{Q}}^\dagger \tilde{\mathbf{K}}) \right).$$

Expanding around $\tilde{\mathbf{Q}}^\dagger \tilde{\mathbf{K}} = \mathbf{0}$, this is approximately:

$$\mathbf{L} \approx \underbrace{\log(\mathbf{P}_{\Delta t}) - \frac{2\kappa}{\nu} \mathbf{P}_{\Delta t}}_{\text{Combined additive bias}} + \underbrace{\frac{2\kappa}{\nu} \mathbf{P}_{\Delta t} \odot \text{Re}(\tilde{\mathbf{Q}}^\dagger \tilde{\mathbf{K}})}_{\text{Precision-modulated dot product}}.$$

When $\mu = 0$, the total covariance becomes a linear function of time:

$$\sigma_V^2(\Delta t) = |\lambda_C|^2 \sigma^2 \Delta t + (\eta^2 + \gamma^2).$$

Without dissipation to bound this growth, the precision $\mathbf{P}_{\Delta t} \propto 1/\sigma_V^2$ vanishes as $\Delta t \rightarrow \infty$.

The resulting additive bias is:

$$\mathbf{B}_{\Delta t} := \log(\mathbf{P}_{\Delta t}) - \frac{2\kappa}{\nu} \mathbf{P}_{\Delta t}$$

The first term is:

$$\mathbf{B}_{\Delta t,1} = -\log(\eta^2 + \gamma^2) - \log \left(1 + \frac{|\lambda_C|^2 \sigma^2}{\eta^2 + \gamma^2} \Delta t \right)$$

Expanding around $\Delta t = 0$ yields the linear approximation:

$$\mathbf{B}_{\Delta t,1} \approx -\log(\eta^2 + \gamma^2) - \frac{|\lambda_C|^2 \sigma^2}{\eta^2 + \gamma^2} \Delta t$$

The second term is:

$$\mathbf{B}_{\Delta t,2} = -\frac{2\kappa}{\nu} \left(|\lambda_C|^2 \sigma^2 \Delta t + (\eta^2 + \gamma^2) \right)^{-1}$$

which rapidly disappears as Δt grows. For $\Delta t \approx 0$, this is:

$$\mathbf{B}_{\Delta t,2} \approx -\frac{2\kappa}{\nu} \left(\frac{1}{\eta^2 + \gamma^2} - \frac{|\lambda_C|^2 \sigma^2}{(\eta^2 + \gamma^2)^2} \Delta t \right)$$

Hence, for small Δt ,

$$\mathbf{B}_{\Delta t} \approx -m \Delta t + \text{const.}, \quad \text{where: } m = \frac{|\lambda_C|^2 \sigma^2}{\eta^2 + \gamma^2} - \frac{2\kappa}{\nu} \frac{|\lambda_C|^2 \sigma^2}{(\eta^2 + \gamma^2)^2}.$$

The first term reflects linear variance growth under Brownian diffusion, while the second arises from the robust (Student- t) likelihood correction. In high-dimensional settings, where typically $\nu = \mathcal{O}(d)$ and $\kappa = (\nu + d)/d = \mathcal{O}(1)$, the second term is suppressed, and the bias is dominated by the diffusion-driven component.

Thus, in the zero-decay and short-time regime, the RFA prior induces an approximately linear distance-dependent bias, analogous in form to the linear penalties used in methods such as ALiBi.

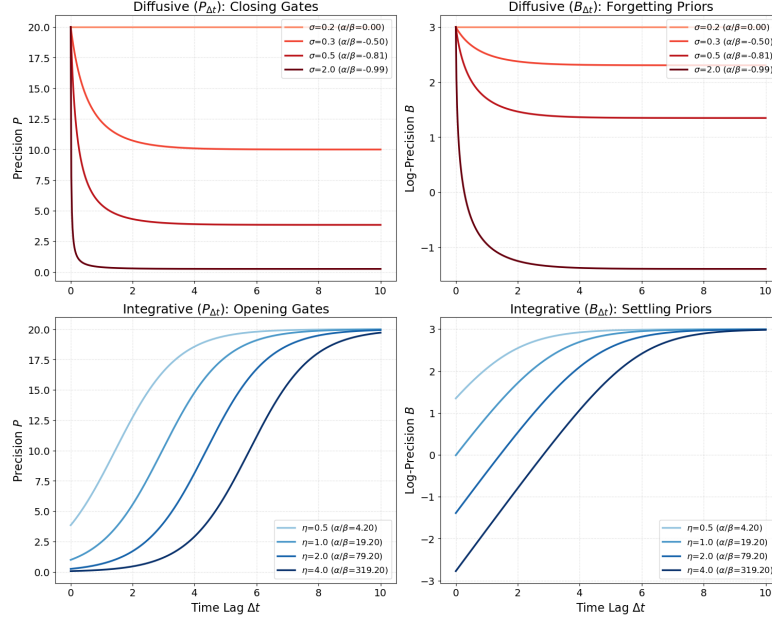


Figure 3. By varying the ratio of steady-state process uncertainty $\tilde{\sigma}^2$ to measurement noise η^2 , RFA heads can specialize into distinct physical regimes: a **diffusive regime** that favors local recency (top row) and an **integrative regime** (bottom row) that filters transient noise to identify stable historical trends. The multiplicative gate $P_{\Delta t}$ controls the selectivity (adaptive gain) of the attention, while the additive bias $B_{\Delta t}$ defines the prior budget allocated to tokens at a given temporal lag.

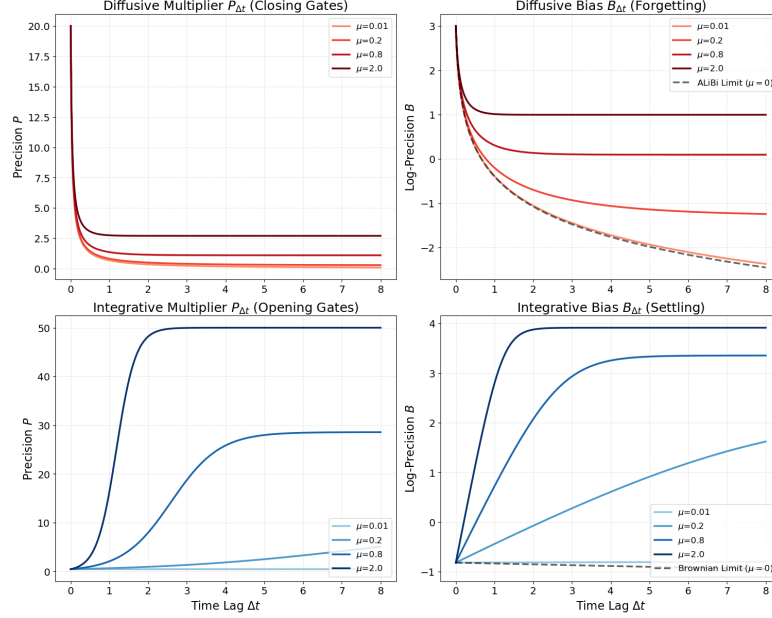


Figure 4. The damping parameter μ dictates the speed of the phase transition. As $\mu \rightarrow 0$, the model recovers non-stationary Brownian dynamics, where precision drops linearly with time. As μ increases, the model enforces stationarity, where the attention bias saturates to a learned global noise floor β , providing a principled mechanism for long-range context retention.

C. Extensions

This section describes extensions and special cases of RFA that preserve its computational and stability guarantees.

C.1. Spectrally Coupled RFA

Isotropic RFA introduces exponential decay to improve extrapolation relative to purely rotational positional encodings. However, a single decay parameter per head applies uniformly across all spectral components represented within that head. Because each attention head implicitly represents a mixture of oscillatory modes, this isotropic treatment cannot distinguish between low-frequency components that encode stable long-range structure and high-frequency components that primarily capture short-range variation. As a result, high-frequency components may persist long enough to contaminate long-range attention, while low-frequency components would remain stable under much weaker decay.

In the zero-rotation limit, ALiBi removes oscillatory positional structure entirely, eliminating high-frequency leakage into long-range attention at the cost of reduced spectral expressivity.

Motivated by this tradeoff, we introduce *Spectrally Coupled RFA* (SC-RFA), which aligns decay rates with spectral scale across attention heads: rather than treating each head as spectrally uniform, we partition the rotational spectrum across heads and couple decay to spectral scale (Fig. 5). Heads associated with higher-frequency rotations are assigned stronger decay, while heads dominated by low-frequency structure use weaker or near-zero decay. This induces a multi-resolution prior in which high-frequency heads act as short-range filters whose influence rapidly diminishes with distance, while low-frequency heads preserve stable long-range dependencies.

In particular, we fix the relative scale between decay and rotation by parameterizing the decay of the k -th head as:

$$\mu_k = b \cdot \max(\omega_k),$$

where ω_k denotes the rotational spectrum assigned to that head and b is a dimensionless damping ratio. This ensures that all heads retain context for a roughly equivalent number of oscillatory cycles, rather than a fixed absolute duration. Setting $b \approx 1$ corresponds to a balanced regime where the signal decay timescale matches the rotational period, effectively suppressing aliasing artifacts beyond a single phase cycle.

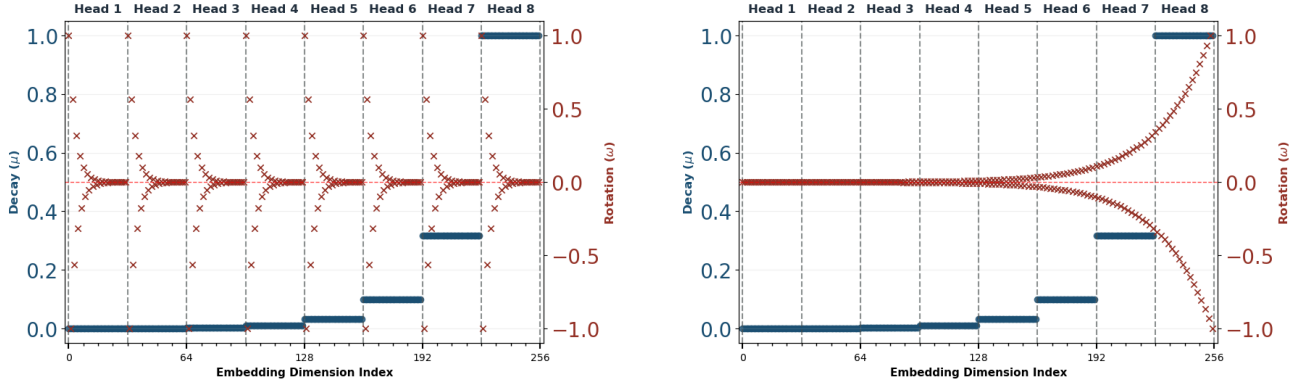


Figure 5. Eigenvalue spectra of rotational positional encodings (with $b=1.0$). *Left:* Standard RoPE with isotropic decay, where each head uses the full range of frequencies (note that we require the eigenvalues to appear in complex conjugate pairs). *Right:* Spectrally Coupled RoPE, where decay increases with rotational frequency, selectively suppressing high-frequency modes while preserving low-frequency structure.

C.2. Inhomogeneous Dynamics and Measurement Bias

The RFA framework is robust to deterministic complexities because, in the diagonalized eigenbasis, their effects collapse analytically into constant bias vectors.

Consider an inhomogeneous linear SDE with a constant drift \mathbf{u} and a measurement model with bias \mathbf{b}_z :

$$d\mathbf{x}(t) = (\mathbf{A}\mathbf{x}(t) + \mathbf{u}) dt + \mathbf{G} d\mathbf{w}(t),$$

$$\mathbf{z}_k = \mathbf{C} \mathbf{x}(t_k) + \mathbf{b}_z + \mathbf{v}(t_k).$$

We assume \mathbf{A} is Hurwitz and \mathbf{A}, \mathbf{C} are invertible. In classical systems theory, the deterministic drift \mathbf{u} is typically eliminated by augmenting the state space with an extra dimension:

$$\mathbf{x}_{\text{aug}} = \begin{bmatrix} \mathbf{x} \\ 1 \end{bmatrix}.$$

This yields a homogeneous SDE:

$$d\mathbf{x}_{\text{aug}}(t) = \mathbf{A}_{\text{aug}} \mathbf{x}_{\text{aug}}(t) dt + \mathbf{G}_{\text{aug}} d\mathbf{w}(t),$$

where \mathbf{A}_{aug} contains the \mathbf{u} term. However, this method is incompatible with the RFA framework because the augmented system matrix \mathbf{A}_{aug} and the augmented process noise covariance $\mathbf{Q}_{\text{aug}} = \mathbf{G}_{\text{aug}} \mathbf{G}_{\text{aug}}^\top$ become singular and are no longer simultaneously diagonalizable. Consequently, the analytic solution to the DLE, which is essential for RFA's $\mathcal{O}(N^2d)$ complexity, fails. For this reason, we must handle the inhomogeneous case directly by seeking a solution that preserves the structure of the underlying homogeneous system.

The SDE can be written in the standard OU form by identifying the equilibrium point μ :

$$d\mathbf{x}(t) = \mathbf{A}(\mathbf{x}(t) - \mu) dt + \mathbf{G} d\mathbf{w}(t), \quad \mu = -\mathbf{A}^{-1}\mathbf{u}.$$

The solution to the SDE, propagating the state forward from $\mathbf{x}(t_j)$ to $\mathbf{x}(t_i)$, is:

$$\mathbf{x}(t_i) = e^{\mathbf{A}\Delta t_{ij}} \mathbf{x}(t_j) + \left(\int_0^{\Delta t_{ij}} e^{\mathbf{A}(\Delta t_{ij} - \tau)} d\tau \right) \mathbf{u} + \int_0^{\Delta t_{ij}} e^{\mathbf{A}(\Delta t_{ij} - \tau)} \mathbf{G} d\mathbf{w}(\tau).$$

Letting $\mathbf{G}_u(\Delta t_{ij}) = \int_0^{\Delta t_{ij}} e^{-\mathbf{A}\tau} d\tau$, the conditional mean of the state at t_i given the state at t_j is:

$$\hat{\mathbf{x}}_{ij} = e^{\mathbf{A}\Delta t_{ij}} \left(\mathbf{x}(t_j) + \mathbf{G}_u(\Delta t_{ij}) \mathbf{u} \right).$$

Letting $\mathbf{u}_s := \mathbf{S}^{-1}\mathbf{u}$, the drift term is:

$$\mathbf{G}_u(\Delta t_{ij})\mathbf{u} = \mathbf{S} \left(\int_0^{\Delta t_{ij}} e^{-\mathbf{A}\tau} d\tau \right) \mathbf{u}_s = \mathbf{S} \left(\frac{\mathbf{I} - e^{-\mathbf{A}\Delta t_{ij}}}{\mathbf{A}} \right) \mathbf{u}_s$$

Hence, the conditional mean in the eigenbasis becomes:

$$\begin{aligned} \hat{\mathbf{x}}_{s,ij} &= e^{\mathbf{A}\Delta t_{ij}} \left(\mathbf{x}_s(t_j) + \left(\frac{\mathbf{I} - e^{-\mathbf{A}\Delta t_{ij}}}{\mathbf{A}} \right) \mathbf{u}_s \right). \\ &= e^{\mathbf{A}\Delta t_{ij}} \left(\mathbf{x}_s(t_j) + \frac{\mathbf{u}_s}{\mathbf{A}} \right) - \frac{\mathbf{u}_s}{\mathbf{A}}. \end{aligned}$$

(where division is element-wise). Including the measurement model:

$$\begin{aligned} \hat{\mathbf{z}}_{s,ij} &= \mathbf{\Lambda}_C e^{\mathbf{A}\Delta t_{ij}} \left(\mathbf{\Lambda}_C^{-1} (\mathbf{z}_{s,j} - \mathbf{b}_{z,s}) + \frac{\mathbf{u}_s}{\mathbf{A}} \right) - \frac{\mathbf{u}_s}{\mathbf{A}} + \mathbf{b}_{z,s} \\ &= e^{\mathbf{A}\Delta t_{ij}} \left(\mathbf{z}_s(t_j) + \boldsymbol{\beta} \right) - \boldsymbol{\beta}, \end{aligned}$$

where $\mathbf{b}_{z,s} = \mathbf{S}^{-1}\mathbf{b}_z$ and $\boldsymbol{\beta} = \frac{\mathbf{\Lambda}_C \mathbf{u}_s}{\mathbf{A}} - \mathbf{b}_{z,s}$. Because the drift contributes only a deterministic mean shift, the covariance evolution—and hence the DLE solution—remains identical to the homogeneous case.

Hence, the drift and measurement bias terms can be accounted for by defining bias terms $\mathbf{b}_q, \mathbf{b}_k, \mathbf{b}_v \in \mathbb{C}^{d \times 1}$ in the input projections defining the queries, keys, and values:

$$\begin{aligned} \mathbf{Q}^u[k, i] &:= \mathbf{Q}[k, i] + \mathbf{b}_Q[k], \quad \mathbf{K}^u[k, i] := \mathbf{K}[k, i] + \mathbf{b}_K[k], \quad \mathbf{V}^u[k, i] := \mathbf{V}[k, i] + \mathbf{b}_V[k], \\ \mathbf{b}_\ell[k] &:= \boldsymbol{\lambda}_{C,k} \frac{\mathbf{u}_\ell[k]}{\boldsymbol{\lambda}_{\ell,k}} + \mathbf{b}_{z,\ell}[k], \quad \ell \in \{\mathbf{Q}, \mathbf{K}, \mathbf{V}\}. \end{aligned}$$

These bias terms correspond to the steady-state offset induced by constant drift in the diagonalized dynamics. This allows the residual tensor to maintain the same form as the homogeneous case, using the biased tensors:

$$\mathcal{R}_{qk}[k, i, j] = \mathbf{Q}^u[k, i] - \mathcal{E}_{qk}[k, i, j] \cdot \mathbf{K}^u[k, j].$$

The attention output is:

$$\begin{aligned} \bar{\mathbf{V}}[k, i] &= \Phi_{\mathbf{v}}[k, i] \cdot \sum_{j \leq i} \mathcal{A}[k, i, j] \cdot \hat{\mathbf{V}}^u[k, j] - \mathbf{b}_{\mathbf{V}}[k] \cdot \sum_{j \leq i} \mathcal{A}[k, i, j] \\ &= \Phi_{\mathbf{v}}[k, i] \cdot \sum_{j \leq i} \mathcal{A}[k, i, j] \cdot \hat{\mathbf{V}}^u[k, j] - \mathbf{b}_{\mathbf{V}}[k] \end{aligned}$$

This final bias can be absorbed into the bias of the output projection: $\mathbf{b}_O := \mathbf{W}_O \mathbf{b}_{\mathbf{V}}$.

Hence, the inhomogeneous SDE with constant drift \mathbf{u} and measurement bias \mathbf{b}_z is structurally equivalent to the homogeneous RFA mechanism, provided the deterministic effects are absorbed into constant bias vectors in the input and output projections ($\mathbf{b}_Q, \mathbf{b}_K, \mathbf{b}_{\mathbf{V}}, \mathbf{b}_O$).

C.3. Stacked Attention Layers as an Unrolled Iterative State Estimator

The robust M-estimator derived in Appendix A.5 is defined implicitly, as the optimal weights w_{ij} depend on the residuals between each historical measurement \mathbf{z}_j and the unknown latent anchor state \mathbf{x}_i . Since \mathbf{x}_i is unobserved, these residuals—and hence the weights—must be computed with respect to the current estimate of the state, obtained by aggregating the propagated measurements, denoted $\bar{\mathbf{z}}_i$.

Because the weights depend on the state estimate, and the state estimate depends on the weights, the solution requires iterative reweighting. This admits an interpretation of each attention layer as one step of an Iteratively Reweighted Least Squares (IRLS)-like procedure: given a state estimate from the previous layer, the current layer recomputes residuals, updates the weights, and produces a refined precision-weighted estimate.

The estimation is performed in the decoupled eigenbasis of the dynamical system, leveraging the diagonal precision matrices Λ_P^Z . Let $\mathbf{z}_{si} := \mathbf{S}^{-1} \mathbf{z}_i$, and initialize: $\hat{\mathbf{z}}_{sii}^{(1)} = \mathbf{z}_{si}$. A single refinement step k updates:

$$\hat{\mathbf{z}}_{sii}^{(k+1)} = \bar{\mathbf{z}}_{si}^{(k)}, \quad \bar{\mathbf{z}}_{si}^{(k)} = \left(\sum_{j \leq i} w_{ij}^{(k)} \boldsymbol{\lambda}_{Pij}^Z \right)^{-1} \odot \sum_{j \leq i} w_{ij}^{(k)} \boldsymbol{\lambda}_{Pij}^Z \odot \hat{\mathbf{z}}_{sij}^{(k)}.$$

Weights are recomputed from the Mahalanobis residuals:

$$w_{ij}^{(k)} := \left(1 + (\boldsymbol{\lambda}_{Pij}^Z)^T |\mathbf{r}_{sij}^{(k)}|^2 / \nu \right)^{-\kappa}, \quad \mathbf{r}_{sij}^{(k)} := \hat{\mathbf{z}}_{sii}^{(k)} - \hat{\mathbf{z}}_{sij}^{(k)}.$$

To improve numerical stability and prevent oscillatory updates, a convex combination (residual connection) may be applied:

$$\hat{\mathbf{z}}_{sii}^{(k+1)} = (1 - \delta) \hat{\mathbf{z}}_{sii}^{(k)} + \delta \bar{\mathbf{z}}_{si}^{(k)}.$$

Stacking L attention layers with shared dynamical structure is therefore equivalent to unrolling L steps of this truncated iterative estimation procedure. Learning can be viewed as learning both the inference procedure and the underlying dynamical prior end-to-end through a fixed number of refinement steps.

C.4. Confidence-Gated Information Fusion

A significant limitation of standard Softmax attention is that the normalization $\sum_j \mathbf{A}_{ij} = 1$ removes the absolute scale of evidence supporting an estimate. In contrast, the Student- t reweighting in RFA fixes an absolute reference through the constant term in $1 + d_{ij}^2 / \nu$. Because d_{ij}^2 depends on the learned residual precision, the scale of precision is identifiable, making sums of unnormalized weights interpretable as accumulated evidence. Consequently, the learned noise parameters $(\tilde{\sigma}^2, \eta^2, \gamma^2)$ are pushed toward meaningful uncertainty levels relative to the residuals, rather than arbitrary rescalings that would otherwise be absorbed by Softmax normalization.

We first quantify the total evidence supporting the latent state at time t_i by computing the aggregate observed Fisher information $\hat{p}_{\text{tot},i}$ for each head:

$$\hat{p}_{\text{tot},i} = \sum_j \tilde{A}_{ij}, \quad \text{where: } \tilde{A}_{ij} := \exp(\mathbf{B}_{\Delta t} - \mathbf{P}_{\Delta t} \odot \|\mathbf{R}_{qk}\|^2)$$

The model must decide whether to trust the SDE-propagated estimate $\bar{\mathbf{V}}_i$ or the raw local observation \mathbf{V}_i . We formulate this as a ratio between the gathered precision \hat{p}_i and a learned prior precision p_{prior} . If $\hat{p}_i \gg p_{\text{prior}}$, the context provides sufficient evidence to override the local noise. We define the gate $\mathbf{g}_i \in (0, 1)^{h \times N}$ using a sigmoid in log-precision space:

$$\mathbf{g}_i = \sigma(p_{\text{scale}} \cdot \log(\hat{p}_i) - \log(p_{\text{prior}}))$$

In this formulation, $p_{\text{prior}} \in (\mathbb{R}^+)^h$ sets the absolute threshold for evidence required to open the gate, while $p_{\text{scale}} \in (\mathbb{R}^+)^h$ dictates the sensitivity to changes in the evidence. We initialize p_{scale} to a small positive value and $\log p_{\text{prior}}$ to a large negative value, so that $\mathbf{g}_i \approx 1$.

The filtered state is then computed as a convex combination:

$$\bar{\mathbf{V}}_i^{\text{fused}} = \mathbf{g}_i \odot \bar{\mathbf{V}}_i + (1 - \mathbf{g}_i) \odot \mathbf{V}_i.$$

This enables the model to act as a self-correcting observer: when the context provides high-precision evidence ($g_i \rightarrow 1$), the model trusts the SDE; if the evidence is insufficient ($g_i \rightarrow 0$), it reverts to the local input.

C.5. Stochastic Latent Sampling

For sequential generation and forecasting, RFA provides a principled marginal for the next-step state by sampling directly from the robust latent estimate and its associated uncertainty.

The filtered state covariance $\Lambda_{\text{filt},i}$ represents the estimation error accumulated across the context window. Given the isotropic constraint, this is the element-wise inverse of the calibrated posterior precision:

$$\Lambda_{\text{filt},i} \approx \hat{p}_i^{-1} \cdot \mathbf{I}.$$

The total predictive covariance combines the propagated estimation error and the intrinsic measurement noise variance of the observation γ^2 :

$$\Lambda_{\text{total}} = \Lambda_{\text{filt},i} + \gamma^2 \mathbf{I},$$

Sampling occurs in the complex latent frame, distributing variance equally between real and imaginary components:

$$\mathbf{z}_i^{\text{sample}} = \bar{\mathbf{z}}_i + \boldsymbol{\epsilon}, \quad \boldsymbol{\epsilon} \sim \mathcal{CN}(0, \Lambda_{\text{total}}), \quad \sigma_{\text{samp}} = \sqrt{\Lambda_{\text{total}}/2}.$$

This produces stochastic latent states consistent with the learned dynamics. Scaling the noise by the aggregate precision increases exploration when contextual uncertainty is high, while the SDE prior maintains structural coherence.

C.6. State Prediction at Future Horizons

To predict Δt_+ steps ahead, we project each historical measurement \mathbf{z}_j through the learned dynamics to the target time $t_i + \Delta t_+$ and then aggregate the projections. Over this interval, the uncertainty grows, requiring *covariance inflation*.

Formally, this modifies the relative-time kernel \mathbf{E} as:

$$\mathbf{E} \rightarrow \exp(-\mu(|t_i - t_j| + \Delta t_+)) = \zeta \exp(-\mu|t_i - t_j|),$$

where $\zeta = e^{-\mu\Delta t_+}$ can be either fixed or learned.

The forward projection of the latent value through the dynamics can be absorbed into the output linear layer, and any additional covariance offset can be absorbed into γ^2 . Effectively, predicting at a future horizon only requires rescaling \mathbf{E} by ζ , leaving the underlying RFA mechanism unchanged.

C.7. Generalized Analytic Priors via Time-Structured Noise

The derivation in Section A.2 assumed white process noise. However, each diagonal DLE is a linear ODE, and allowing the noise injection rate $q_k(t)$ to vary in time yields a richer class of analytic priors. For each mode k with decay $\mu_k = -\text{Re}(\lambda_k)$, the covariance satisfies:

$$\frac{d}{d\Delta t} \lambda_{V,k}(\Delta t) = -2\mu_k \lambda_{V,k}(\Delta t) + q_k(\Delta t), \quad \lambda_{V,k}(0) = 0.$$

The unique solution is given by the convolution of the mode-specific noise source $q_k(s)$ with the system's exponential impulse response:

$$\lambda_{V,k}(\Delta t) = \int_0^{\Delta t} e^{-2\mu_k(\Delta t-s)} q_k(s) ds.$$

To ensure $\lambda_{V,k}(\Delta t)$ remains analytically tractable and computable in parallel, we restrict the noise source to the class of functions closed under exponential convolution: the complex exponentials. Letting $q_k(s) = \sum_j c_j e^{\gamma_j s}$ for $c_j, \gamma_j \in \mathbb{C}$, the integral yields a weighted sum of exponential differences:

$$\lambda_{V,k}(\Delta t) = \text{Re} \left[\sum_j c_j \left(\frac{e^{\gamma_j \Delta t} - e^{-2\mu_k \Delta t}}{2\mu_k + \gamma_j} \right) \right].$$

This structure allows the model to analytically represent an oscillatory precision prior, which may help regularize the model by offloading predictable noise variability into the prior, reducing the burden on the data-dependent attention weights.

D. Implementation

D.1. Complex-valued Computations

RFA is formulated in a complex latent space to represent oscillatory dynamics. In practice, all operations are implemented using real-valued tensors by stacking real and imaginary components, i.e., via the standard isomorphism $\mathbb{C}^d \cong \mathbb{R}^{2d}$, so that complex multiplications and projections reduce to ordinary real-valued linear algebra.

We denote a complex linear layer by $\mathcal{L}(\cdot)$. For an input $\mathbf{x} = [\mathbf{x}_r, \mathbf{x}_i]^\top$ with $\mathbf{x}_r, \mathbf{x}_i \in \mathbb{R}^d$, the layer computes:

$$\mathcal{L}(\mathbf{x}) = \begin{bmatrix} \mathbf{W}_r & -\mathbf{W}_i \\ \mathbf{W}_i & \mathbf{W}_r \end{bmatrix} \mathbf{x} + \begin{bmatrix} \mathbf{b}_r \\ \mathbf{b}_i \end{bmatrix},$$

Here $\mathbf{W}_r, \mathbf{W}_i \in \mathbb{R}^{d \times d}$ are the real and imaginary components of the weight matrix and $\mathbf{b}_r, \mathbf{b}_i \in \mathbb{R}^d$ the bias. This is equivalent to multiplication by a complex matrix $\mathbf{W} = \mathbf{W}_r + i\mathbf{W}_i$ with bias $\mathbf{b} = \mathbf{b}_r + i\mathbf{b}_i$, while remaining in the real domain.

Assuming the inputs and outputs are purely real, only the real-input columns of the input projections and the real-output columns of the output projections are required:

$$\mathcal{L}^{\mathbb{R} \rightarrow \mathbb{C}}(\mathbf{x}_r) := \begin{bmatrix} \mathbf{W}_r \\ \mathbf{W}_i \end{bmatrix} \mathbf{x}_r + \begin{bmatrix} \mathbf{b}_r \\ \mathbf{b}_i \end{bmatrix}.$$

$$\mathcal{L}^{\mathbb{C} \rightarrow \mathbb{R}}(\mathbf{x}) := [\mathbf{W}_r \quad -\mathbf{W}_i] \mathbf{x} + \mathbf{b}_r.$$

Hence, both projections may be implemented using standard real-valued linear layers in \mathbb{R}^{2d} .

We define queries, keys, and values using:

$$\mathbf{Q} = \mathcal{L}_{\mathbf{Q}}^{\mathbb{R} \rightarrow \mathbb{C}}(\mathbf{Z}), \quad \mathbf{K} = \mathcal{L}_{\mathbf{K}}^{\mathbb{R} \rightarrow \mathbb{C}}(\mathbf{Z}), \quad \mathbf{V} = \mathcal{L}_{\mathbf{V}}^{\mathbb{R} \rightarrow \mathbb{C}}(\mathbf{Z})$$

We define cosine and sine matrices:

$$\mathbf{C}[k, i] = \cos(\omega_k t_i), \quad \mathbf{S}[k, i] = \sin(\omega_k t_i)$$

Complex rotations are applied as:

$$\tilde{\mathbf{Q}}^\top = \begin{bmatrix} \tilde{\mathbf{Q}}_r^\top \\ \tilde{\mathbf{Q}}_i^\top \end{bmatrix} = (\tilde{\Phi}^-)^\top \odot \mathbf{Q}^\top = \begin{bmatrix} \mathbf{C} \odot \mathbf{Q}_r^\top + \mathbf{S} \odot \mathbf{Q}_i^\top \\ \mathbf{C} \odot \mathbf{Q}_i^\top - \mathbf{S} \odot \mathbf{Q}_r^\top \end{bmatrix},$$

and likewise for keys and values. This is algebraically identical to RoPE.

To ensure the underlying system matrix \mathbf{A} is real-valued, we enforce that latent frequencies appear in complex conjugate pairs:

$$\omega = \{\omega_1, -\omega_1, \dots, \omega_{d/2}, -\omega_{d/2}\},$$

The Mahalanobis distance requires the real part of the complex inner product,

$$\text{Re}(\tilde{\mathbf{Q}}^\dagger \tilde{\mathbf{K}}) = \tilde{\mathbf{Q}}_r^\top \tilde{\mathbf{K}}_r + \tilde{\mathbf{Q}}_i^\top \tilde{\mathbf{K}}_i = \begin{bmatrix} \tilde{\mathbf{Q}}_r^\top & \tilde{\mathbf{Q}}_i^\top \end{bmatrix} \begin{bmatrix} \tilde{\mathbf{K}}_r \\ \tilde{\mathbf{K}}_i \end{bmatrix}.$$

This is implemented as a single real matrix multiplication in \mathbb{R}^{2d} .

Value aggregation, $\tilde{\mathbf{V}}$, is computed in the \mathbb{R}^{2d} domain. The real-valued attention matrix \mathbf{A} is applied identically to both the real and imaginary components of the complex-rotated values:

$$\mathbf{M}^\top = \begin{bmatrix} \mathbf{A} \tilde{\mathbf{V}}_r^\top \\ \mathbf{A} \tilde{\mathbf{V}}_i^\top \end{bmatrix}.$$

The inverse rotation yields:

$$\bar{\mathbf{Z}}_v^\top = (\tilde{\Phi}^+)^{\top} \odot (A\tilde{\mathbf{V}}^\top) = \begin{bmatrix} \mathbf{C} \odot \mathbf{M}_r^\top - \mathbf{S} \odot \mathbf{M}_i^\top \\ \mathbf{C} \odot \mathbf{M}_i^\top + \mathbf{S} \odot \mathbf{M}_r^\top \end{bmatrix}$$

The final output is projected back to the real domain using the $\mathcal{L}^{\mathbb{C} \rightarrow \mathbb{R}}$ layer:

$$\bar{\mathbf{Z}} = \mathcal{L}_O^{\mathbb{C} \rightarrow \mathbb{R}}(\bar{\mathbf{V}}) = [\mathbf{W}_r \quad -\mathbf{W}_i] \bar{\mathbf{V}} + \mathbf{b}_r \in \mathbb{R}^{d \times N}.$$

All components of RFA are therefore implemented using standard real-valued operations.

D.2. Initialization

The RFA model initializes complex projections and dynamics to cover multiple temporal scales and ensure numerical stability.

Isotropic Complex Projections. Complex weights $\mathbf{W} = \mathbf{W}_r + i\mathbf{W}_i$ are represented in \mathbb{R}^{2d} and initialized isotropically:

$$\mathbf{W}_{ij} = M_{ij} \begin{bmatrix} \cos(\phi_{ij}) \\ \sin(\phi_{ij}) \end{bmatrix}, \quad M_{ij} \sim \text{Rayleigh}\left(\sqrt{\frac{1}{d_{\text{in}} + d_{\text{out}}}}\right), \quad \phi_{ij} \sim \mathcal{U}(0, 2\pi).$$

Output projections (\mathbf{W}_O) are scaled by $1/\sqrt{2}$ to preserve variance when converting back to real space.

Dynamics and Head Specialization. In SC-RFA, we define a global frequency bank and partition it across heads such that each head specializes in a distinct spectral band. To ensure stability, the decay rate μ_h is coupled to the head's maximum frequency: $\mu_h = b \cdot \max(\omega_h)$. In RFA (non spectrally coupled), we use the same spread of decay rates, though each head receives the full range of angular frequencies. In our primary models (M1-M2.6), we use a damping coefficient $b = 0.05$, prioritizing near-field accuracy rather than long-context extrapolation. We reserve a fraction of heads (2 out of 8) with $\mu = 0$ to give the model the capacity to learn lossless, infinite-horizon integrators.

Noise and Robustness. We initialize a constant steady-state uncertainty $\tilde{\sigma}$ across heads, i.e. $\sigma \propto \mu$. We initialize measurement noise (η^2, γ^2) such that the model begins in the integrative regime ($\eta^2 > \tilde{\sigma}^2$), to preserve long-range gradient flow early in training.

The Student- t degrees of freedom ν are initialized as a multiple of head dimension d . We set $\nu = 4d$, placing the model in a quasi-Gaussian regime during the initial phase of training. This provides a broad “trusting prior” that prevents the premature rejection of tokens while the Query-Key representations are still unoptimized.

Note. In our implementation, σ^2 was learned directly. A potentially preferable parameterization is in terms of $\tilde{\sigma}^2 := |\lambda_C|^2 \sigma^2 / (2\mu)$, which decouples the steady-state variance floor from the dissipation rate μ and may improve numerical conditioning. We also suggest initializing near the boundary between the diffusive and integrative regimes ($\alpha = 0$), particularly for heads with small decay rates, as a reasonable default when no prior on the noise regime is available.

D.3. Algorithm

Algorithm 1 details the implementation of Isotropic RFA.

(**Note:** We use \oplus to denote broadcast addition.)

Algorithm 1 Robust Filter Attention (Isotropic; Single Head)

Input: Input sequence $Z \in \mathbb{R}^{d \times N}$

Definitions:

Linear layers: $\mathcal{L}_Q^{\mathbb{R} \rightarrow \mathbb{C}}, \mathcal{L}_K^{\mathbb{R} \rightarrow \mathbb{C}}, \mathcal{L}_V^{\mathbb{R} \rightarrow \mathbb{C}}, \mathcal{L}_O^{\mathbb{C} \rightarrow \mathbb{R}}$; dynamics/noise variance parameters: $\mu', \omega', \sigma', \eta', \gamma'$; robustness parameter ν ; Softmax temperature τ_s .

Constants: Causal mask $M_{\text{causal}} \in \{0, -\infty\}^{N \times N}$; stability constant ϵ .

Enforce Conjugate Symmetry: $\omega \in \{\omega'_1, -\omega'_1, \dots, \omega'_{d/2}, -\omega'_{d/2}\}$.

Ensure positive noise/decay parameters:

$\{\mu, \tilde{\sigma}^2, \eta^2, \gamma^2\} \leftarrow \text{softplus}(\{\mu', \sigma', \eta', \gamma'\}) + \epsilon$

Input projections:

$(\text{Re}(Q), \text{Im}(Q)) \leftarrow \mathcal{L}_Q^{\mathbb{R} \rightarrow \mathbb{C}}(Z)$,

$(\text{Re}(K), \text{Im}(K)) \leftarrow \mathcal{L}_K^{\mathbb{R} \rightarrow \mathbb{C}}(Z)$,

$(\text{Re}(V), \text{Im}(V)) \leftarrow \mathcal{L}_V^{\mathbb{R} \rightarrow \mathbb{C}}(Z)$

Decay and rotation kernels: $E[i, j] = e^{-\mu|t_i - t_j|}, \quad \tilde{\Phi}^+[k, i] = e^{i\omega_k t_i}, \quad \tilde{\Phi}^-[k, i] = e^{-i\omega_k t_i}$

Covariance kernel: $V_{\Delta t}[i, j] = \tilde{\sigma}^2(1 - E^2[|t_i - t_j|]) + \eta^2 E^2[|t_i - t_j|] + \gamma^2$

Query/Key/Value Rotations: $\tilde{Q}[k, i] = \tilde{\Phi}^- \odot Q[k, i], \quad \tilde{K}[k, j] = \tilde{\Phi}^- \odot K[k, j], \quad \tilde{V}[k, i] = \tilde{\Phi}^- \odot V[k, i]$

Squared residuals: $\|R_{qk}\|^2 = \|Q\|_{\text{cols}}^2 \oplus (E^2 \odot \|K\|_{\text{rows}}^2) - 2E \odot \text{Re}(\tilde{Q}^\dagger \tilde{K})$

Additive & Multiplicative Bias: $B_{\Delta t} = -\log(V_{\Delta t}), \quad P_{\Delta t} = 1/V_{\Delta t}$.

Logits: $L = B_{\Delta t} - \kappa \log \left(1 + \frac{1}{\nu} P_{\Delta t} \odot \|R_{qk}\|^2 \right)$, where $\kappa = \frac{\nu+d}{d}$.

Attention matrix: $\hat{A}[i, j] = \text{Softmax}_j(\tau_s L[i, j] + M_{\text{causal}}), \quad A = \hat{A} \odot E$

Output with value counter-rotations: $\bar{V} = \tilde{\Phi}^+ \odot (\tilde{V} A^\top)$

Output projection: $\text{Re}(\bar{Z}) \leftarrow \mathcal{L}_O^{\mathbb{C} \rightarrow \mathbb{R}}(\text{Re}(\bar{V}), \text{Im}(\bar{V}))$

Return: $\text{Re}(\bar{Z})$

Our current implementation is written in high-level PyTorch and incurs an approximately $2\times$ training overhead relative to PyTorch's optimized scaled dot-product attention backend.

E. Experimental Details and Ablations

E.1. Experimental Setup

Architecture and Model Configuration All experiments were conducted using a 6-layer decoder-only Transformer architecture. We set the model dimension to $d_{\text{model}} = 256$ with $h = 8$ attention heads. The attention mechanism maps the model dimension to a total latent dimension of 512 via the $d \times 2d$ query, key, and value projections (split into $d_k = 64$ per head), while the $2d \times d$ output projection maps back down to 256.

We employ a Pre-Norm configuration using Layer Normalization. The position-wise Feed-Forward Network utilizes an expansion factor of 4. To optimize the parameter budget, we implement weight tying between the token embedding layer and the final linear output head. We use the GPT-2 byte-pair encoding (BPE) tokenizer with a vocabulary size of 50,257 for all language modeling experiments.

To ensure a fair comparison, RFA models and the baselines (RoPE and ALiBi) were designed with near-identical parameter counts. RFA introduces only a small set of scalar coefficients per head to parameterize the SDE-based drift (μ), noise ($\tilde{\sigma}^2, \eta^2, \gamma^2$), and robustness (ν, τ_s). Hence, the RFA models match the baseline parameter count (19.36M), with only a 0.02% increase due to additional scalar coefficients.

Training and Optimization Protocol Models were trained for 15 epochs using the Adam optimizer. We utilized a OneCycleLR scheduler with cosine annealing and a 5% warmup period. For RFA models, we adopted a decoupled optimization strategy to ensure the stability of the SDE coefficients:

- **Feature Weights:** Peak LR of 1×10^{-3} with momentum $\beta_1 = 0.9$ (same as in baselines).
- **SDE Coefficients:** Peak LR of 5×10^{-4} with no momentum ($\beta_1 = 0.0$) and a higher $\epsilon = 10^{-7}$ to prevent numerical instability and oscillatory updates.

We apply global gradient clipping at a threshold of 1.0. For the RFA-specific physics parameters, we apply a stricter local clipping threshold of 1×10^{-4} as a precaution. All models were trained on the WikiText-103 and BabyLM-2025 datasets using a standard causal language modeling objective.

E.2. Model Variants and Ablation Design

This section presents a series of ablations designed to isolate the contributions of RFA’s core components.

We distinguish between three categories of models:

1. Positional baselines used in the main text (B1–B4),
2. Final RFA variants evaluated in Section 4 (M1–M2), and
3. Structural diagnostic ablations (M2.1–M2.6), which progressively remove components of the filtering formulation to test necessity and failure modes. These models are not intended as competitive models, but rather as mechanistic probes of stability and extrapolation behavior.

Baselines:

- **B1: Standard Transformer + RoPE.** Dot-product attention with rotary positional embeddings (Su et al., 2024). Applies $d \rightarrow 2d \rightarrow d$ projections to match RFA parameterization.
- **B2: Standard Transformer + ALiBi.** Dot-product attention with linear distance bias (Press et al., 2022). Tests whether static geometric penalties are sufficient for stability.
- **B3: Decayed RoPE.** RoPE with an additional exponential decay applied to attention scores per-head, as in RFA, testing whether explicit dissipation alone suffices in the absence of uncertainty modeling.
- **B4: Spectrally Coupled RoPE (SC-RoPE).** Frequency-partitioned RoPE with head-wise decay schedules, testing whether multi-scale geometric heuristics alone can recover SC-RFA’s stability.

Primary RFA Models:

- **M1: Isotropic RFA.** Isotropic RFA as described in Algorithm D.3, replacing the attention module in a standard Transformer.
- **M2: Spectrally Coupled RFA (SC-RFA).** M1 with explicit coupling between rotation frequencies and decay rates, yielding a multi-resolution filtering prior.

Structural Diagnostic Ablations: These ablations progressively remove components of the filtering formulation, starting from the full SC-RFA model (M2) and simplifying toward standard attention. Their purpose is to isolate which mechanisms are required for stable extrapolation.

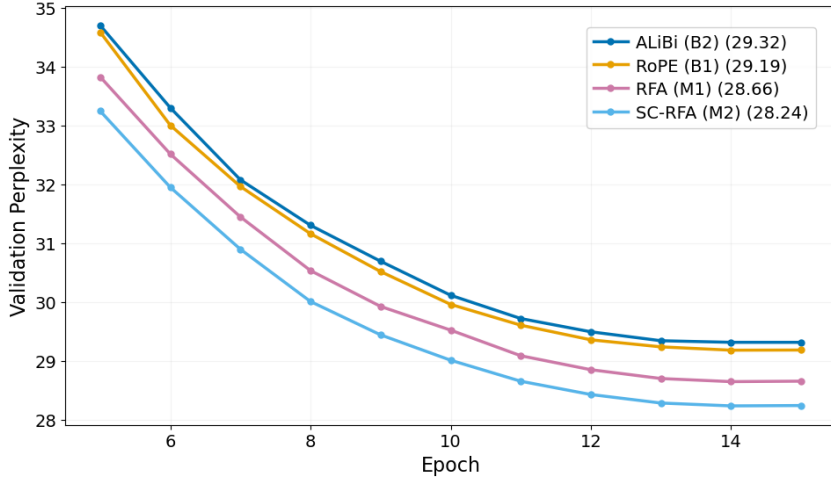
- **M2.1: Exponential Kernel.** M2 with Student’s $-t$ influence function replaced by an exponential weighting, i.e., $w_{ij} = \exp(-d_{ij}^2/\nu)$. This isolates the effect of heavy-tailed robust reweighting under the same dynamical precision prior.
- **M2.2: Flat Precision Prior.** M2 with noise parameters removed so that $\mathbf{P}_{\Delta t}$ is constant across time lag. Tests whether dynamics alone suffice without uncertainty accumulation.
- **M2.3: No Multiplicative Gate.** M2 with the multiplicative gating term $\mathbf{P}_{\Delta t}$ set to a constant, to test the impact of the additive bias $\mathbf{B}_{\Delta t}$ in isolation.
- **M2.4: No Value Frame Alignment.** M2 without value rotation and counter-rotation, testing the necessity of aggregating in a shared temporal frame.
- **M2.5: No Rotational Dynamics.** M2 without rotations applied to queries, keys, or values, isolating the effect of decay-only dynamics.
- **M2.6: Unitary Dot-Product Limit.** No decay, no process or measurement noise, and no magnitude normalization, so that attention weights reduce to normalized complex dot products between unit-modulus rotated embeddings. This yields a unitary, phase-only attention mechanism analogous to RoPER (Harik, 2023).

F. Additional Experimental Results

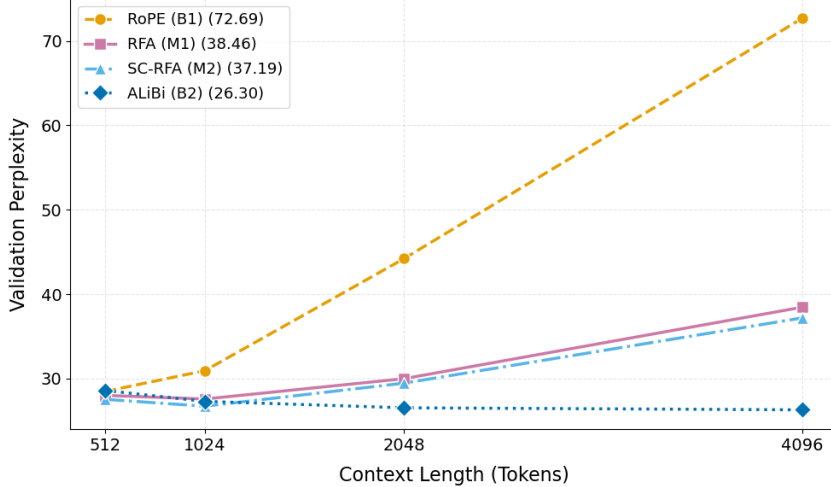
F.1. Training Dynamics and Extrapolation Behavior

To assess learning efficiency, we track validation perplexity throughout training (Fig. 6a). Both RFA (M1) and SC-RFA (M2) converge faster than RoPE (B1) and ALiBi (B2), reaching lower validation perplexity earlier in training. This suggests that the SDE-based prior provides a more informative inductive bias for latent state estimation than purely geometric positional encodings. SC-RFA consistently outperforms Isotropic RFA, indicating that spectral coupling improves both optimization and final accuracy.

Figure 6b visualizes training dynamics and length extrapolation trends corresponding to the tabulated results in Section 4. RFA variants converge faster and degrade more gradually with context length than RoPE, while ALiBi remains stable due to its enforced locality.



(a) Validation perplexity over training epochs.



(b) Test perplexity under length extrapolation beyond the training window (512 tokens).

Figure 6. Training dynamics and length extrapolation on WikiText-103. RFA variants converge faster during training and degrade more gradually with increasing context length than RoPE, while ALiBi remains stable due to enforced locality.

Figure 7 shows the sensitivity analysis over damping values b reported in Table 2. Increasing damping improves long-range stability by suppressing high-frequency propagation, but excessively large damping degrades short-range modeling. The optimal trade-off among the values we tested occurs near $b \approx 5 \times 10^{-2}$, which maximizes medium-range context utilization

while preserving stability.

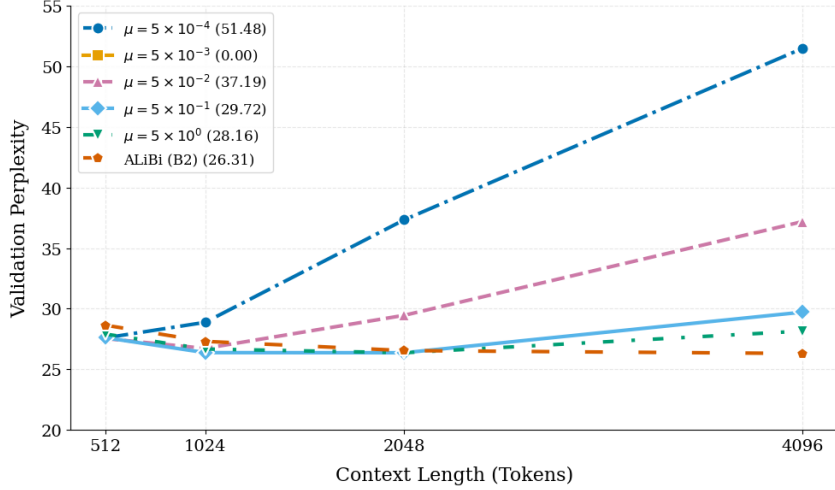


Figure 7. Impact of the Damping Coefficient b on Length Extrapolation. Perplexity curves for varying b demonstrate that higher damping coefficient values effectively stabilize long-range integration.

F.2. Parameter Dynamics in RFA

Learned measurement and process noise parameters over the course of training are shown in Fig. 8 for the last layer of both RFA (M1) and SC-RFA (M2). The learned noise parameters reveal structured head specialization and adaptive uncertainty calibration. Distinct trajectories in query and key noise parameters indicate that different heads self-organize into separate signal-to-noise regimes. We plot inverse temperature τ_s and robustness parameter ν/d in Fig. 9.

In general, lower-decay heads tend to converge to lower measurement noise variance (η^2, γ^2), lower robustness parameter (ν/d), and higher inverse temperature τ_s , consistent with stable long-range integration, while higher-decay heads tend to tolerate larger measurement noise and focus on local structure.

Intermediate heads tend to converge to the highest measurement noise variance, lowest steady-state process uncertainty, and strongest robustness, consistent with modeling heterogeneous and noisy mid-range structure, while extreme short- and long-range heads tend to remain more tolerant to outliers.

The spectrally coupled model (M2, SC-RFA) exhibits lower average query and key noise variance and more clustered trajectories across heads.

When initialized in the diffusive regime, we observed that higher-decay heads consistently transitioned into the integrative regime ($\alpha > 0$), while the lowest-decay heads remained diffusive (Fig. 10).

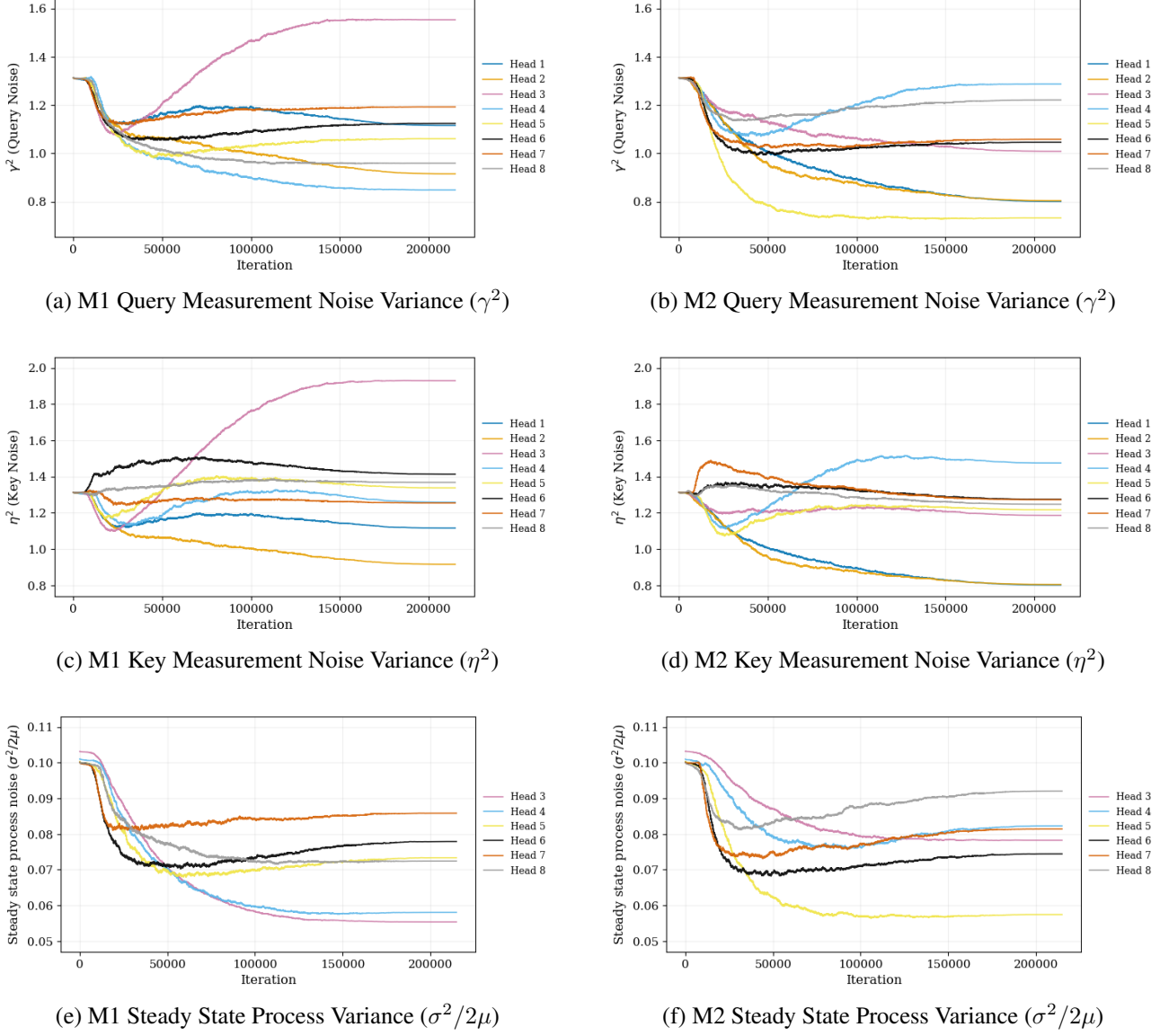


Figure 8. **Measurement and Process Noise Parameters Comparison.** Query and key measurement noise variance and state process variance for M1 and M2, over the course of training. (Note that $\tilde{\sigma}^2$ is undefined for heads 0 and 1, with $\mu = 0$.)

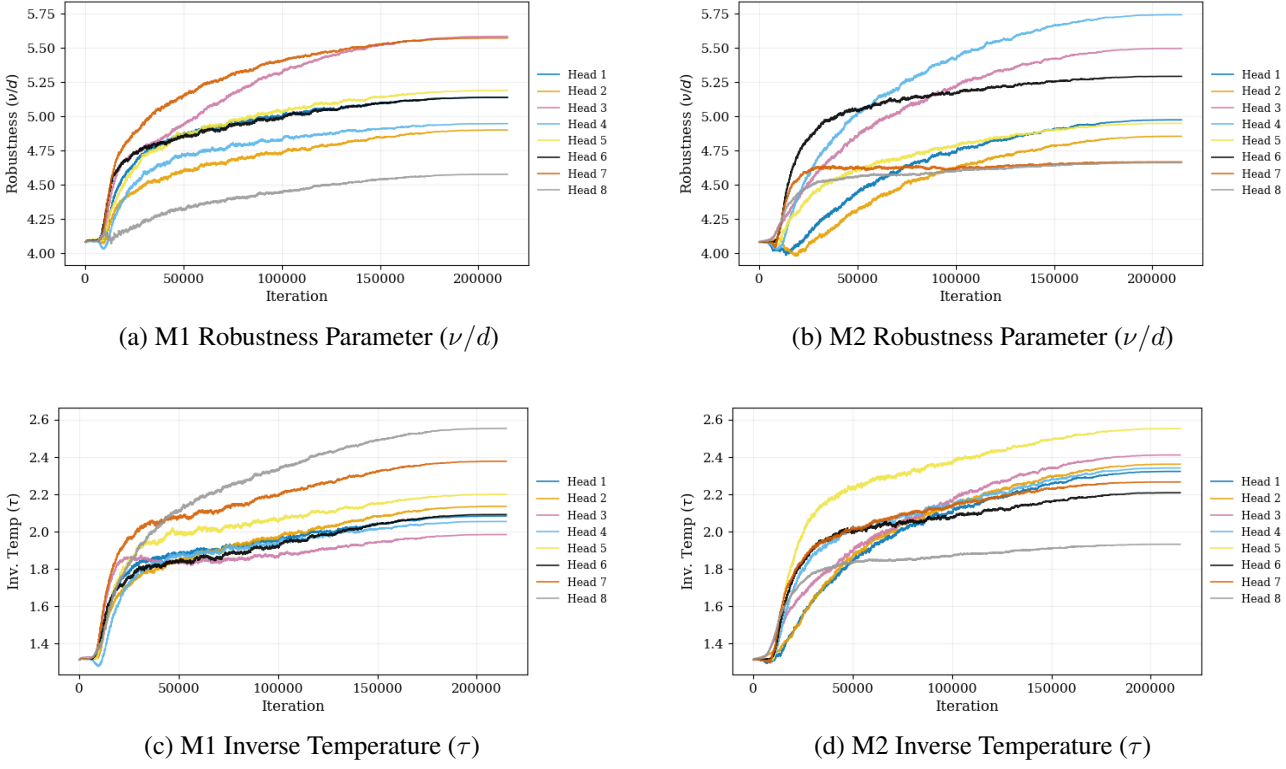


Figure 9. **Robustness and inverse temperature.** Robustness parameter and inverse temperature for M1 and M2, over the course of training.

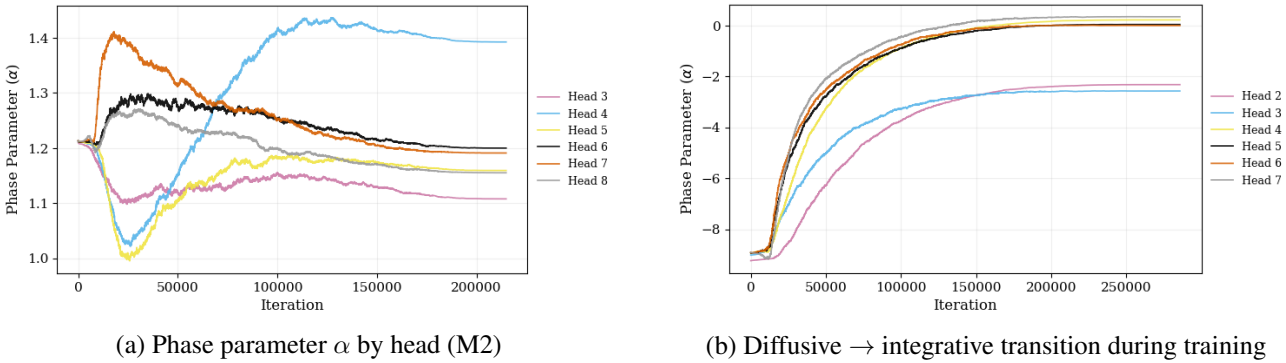


Figure 10. **Integrative dynamics in SC-RFA.** (a) Phase parameter (α) under standard initialization, showing specialization across heads. (b) When initialized in the diffusive regime ($\alpha < 0$), most heads transitioned into the integrative regime ($\alpha > 0$) during training, while the two lowest-decay heads remained diffusive. (Note that α is undefined for heads 0 and 1, with $\mu = 0$.)

F.3. Analysis of Attention Matrices

We plot attention matrices at a context length of 4096 to visualize long-range behaviors induced by each positional prior: the baselines RoPE (B1) (Fig 11) and ALiBi (B2) (Fig 12); and the RFA (M1) (Fig 13) and SC-RFA (M2) (Fig 14) models. We use attention matrices from the last layer of each model.

Note: For the RFA models, for improved visualization, we plot the unattenuated attention matrix \hat{A} rather than the physical (decayed) attention matrix $A := \hat{A} \odot E$ (see Appendix B.3.3).

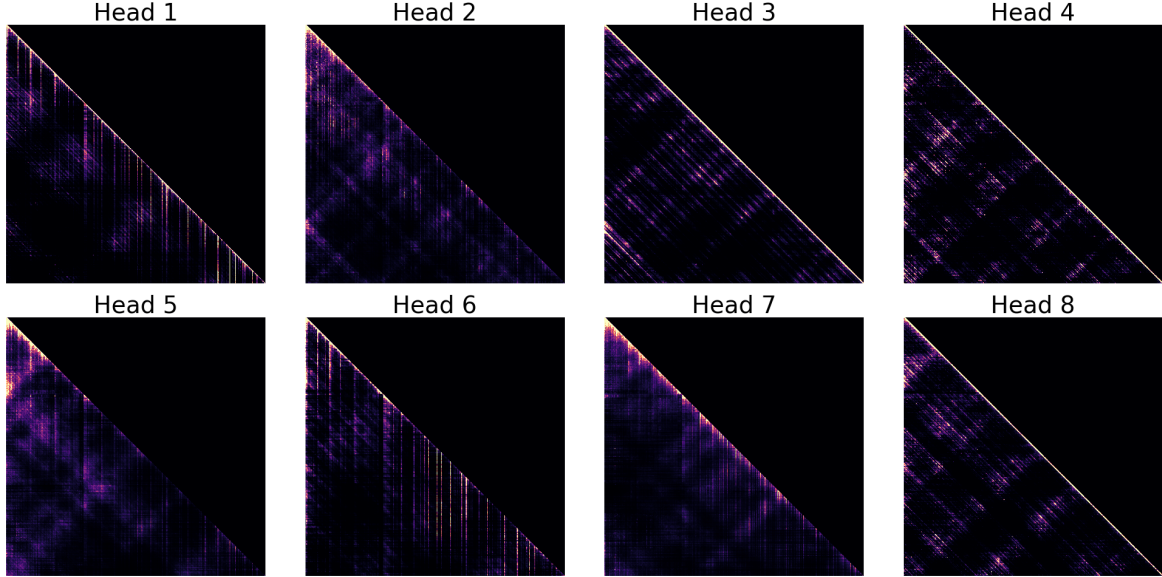


Figure 11. Baseline RoPE Transformer (B1) at $L = 4096$: Attention map exhibits persistent checkerboard structure.

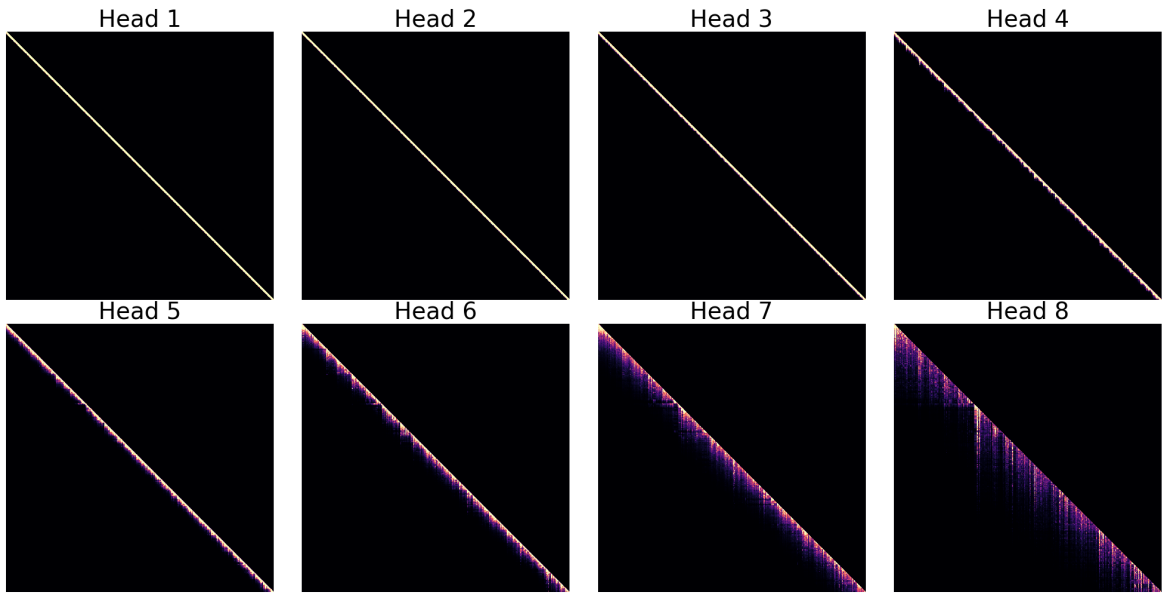


Figure 12. ALiBi Transformer (B2) at $L = 4096$: Attention map remains tightly localized to the diagonal across all heads, with only modest widening in higher heads. Long-range structure is suppressed rather than integrated.

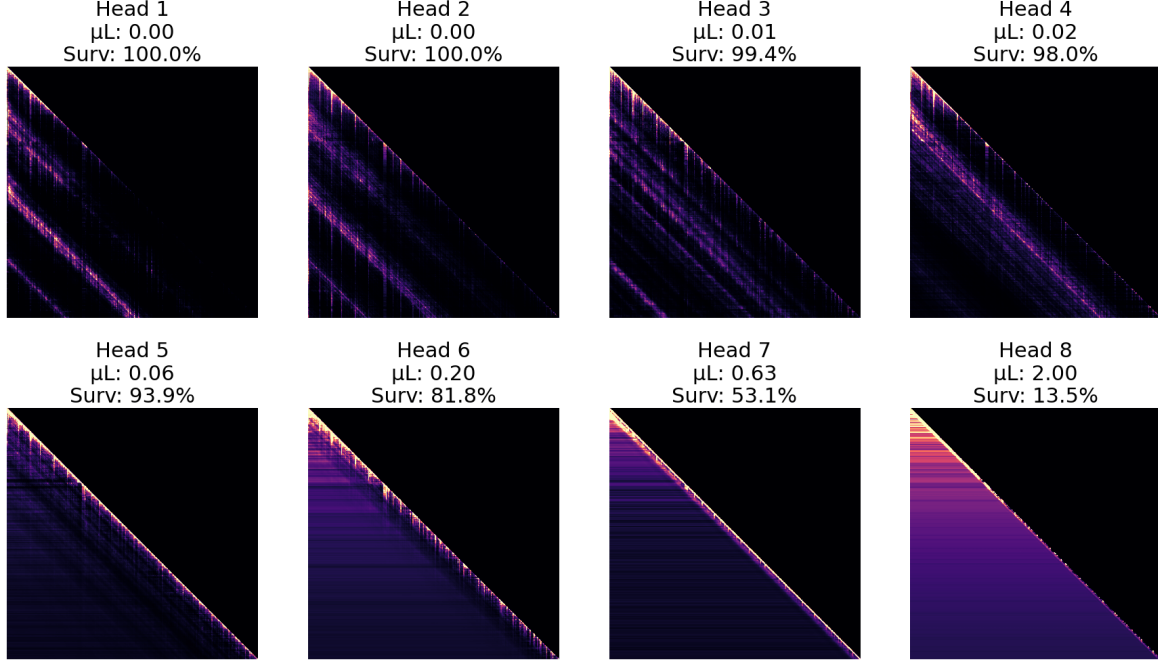


Figure 13. Robust Filter Attention (M1) at $L = 4096$: RFA demonstrates emergent scale separation and dynamical consistency. Periodic bands are clearly visible. High-decay heads concentrate focus on the local diagonal, while low-decay heads exhibit the **Integrative (Opening Gate)** regime: the bottom-right corner near the diagonal is suppressed as the model waits for the SDE dynamics to suppress initial measurement noise before assigning high precision to the state estimate.

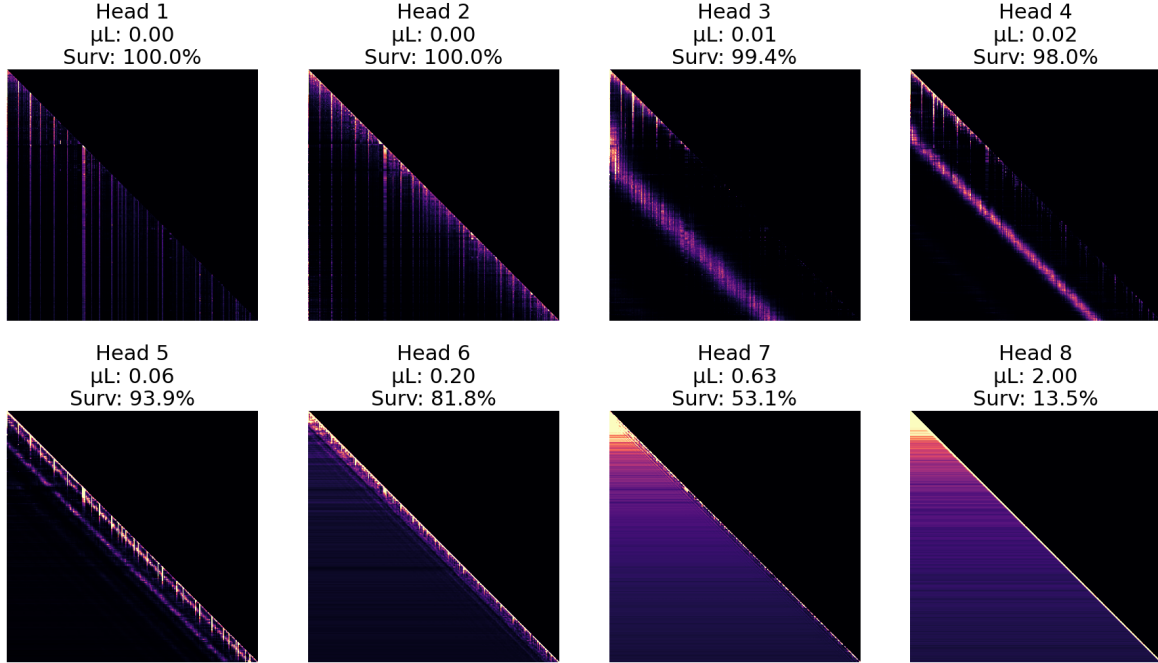


Figure 14. Spectrally-Coupled RFA (M2, $b = 0.05$) at $L = 4096$. Frequency-dependent damping ($\mu_h = b \cdot \omega_{h,\max}$) substantially alters long-range attention structure. SC-RFA has fewer periodic bands than RFA. Heads 3-5 each have only a single band, which become narrower and moves closer to the diagonal as decay increases.

The attention maps for RoPE exhibit persistent “checkerboard” artifacts and high-frequency oscillations that remain visible even at large temporal offsets. A possible explanation is that, because RoPE implicitly assumes zero decay, high-frequency spectral components remain unattenuated into the far-field context, and may fail to settle into a smooth summary, potentially contributing to the chaotic, non-local attention patterns observed at long distances.

In ALiBi, attention remains strongly localized to the diagonal across all heads, reflecting ALiBi’s fixed distance-based bias. Higher heads exhibit modestly broader receptive fields, but attention never transitions to a global integrative regime: long-range context is suppressed rather than accumulated, yielding stable extrapolation through enforced locality rather than dynamical state propagation.

The periodic banding visible in M1 and M2 is more clearly visible than in RoPE. By rotating values into a stationary frame before aggregation, RFA preserves dynamical phase relationships. In contrast, RoPE aggregates in the observation frame, potentially causing cumulative phase lag and destructive interference across time.

In some low-decay heads, RFA exhibits a distinct “opening gate” behavior where the attention weight for a given query is not maximal at the immediate diagonal ($\Delta t = 0$), but instead peaks at a specific historical lag. This is visible as a dark band directly following the diagonal, which then transitions into a bright region of high-precision attention. This is visible, for example, in heads 3 and 4 of SC-AFA.

Coupling decay to frequency ($\mu_h = b \cdot \omega_{h,\max}$) causes different heads to specialize at different time scales. Compared to M1, where heads mix many oscillatory patterns, intermediate heads in M2 (Heads 3–5) show fewer, sharper periodic bands. As frequency (and thus decay) increases, these bands become narrower and concentrate closer to the diagonal. For high-decay heads (6 and 7), structure in the attention map is confined to a narrow band near the diagonal, while the flat horizontal bands indicate that the model has reached its precision floor. By head 8, the attention map becomes effectively diagonal.

Spectral coupling in SC-RFA (M2) restores clean vertical attention lines corresponding to retrieval of salient “anchor” tokens. In purely rotational models like RoPE, such content-based signals are often obscured by checkerboard aliasing, where high-frequency positional jitter propagates without decay and creates widespread interference. By selectively damping fast frequencies, SC-RFA suppresses this positional noise, allowing low-frequency heads (Heads 1–3) to lock onto globally significant tokens and maintain high-precision connections over long horizons.

In SC-RFA (M2), attention maps exhibit clear vertical structures corresponding to repeated retrieval of salient “anchor” tokens. This suggests that by coupling higher frequencies with stronger decay, SC-RFA reduces the influence of rapidly varying components, allowing lower-frequency heads (Heads 1–3) to more consistently attend to globally relevant tokens over long contexts. Taken together, these patterns suggest that RFA models learn physically meaningful multi-scale filtering behavior, rather than merely exploiting dataset-specific positional correlations.